

## Article

# Active Site Coupling in PDE:PKA Complexes Promotes Resetting of Mammalian cAMP Signaling

Srinath Krishnamurthy,<sup>1,2</sup> Balakrishnan Shenbaga Moorthy,<sup>1</sup> Lim Xin Xiang,<sup>1</sup> Lim Xin Shan,<sup>1</sup> Kavitha Bharatham,<sup>3</sup> Nikhil Kumar Tulsian,<sup>1</sup> Ivana Mihalek,<sup>3</sup> and Ganesh S. Anand<sup>1,2,\*</sup>

<sup>1</sup>Department of Biological Sciences and <sup>2</sup>Mechanobiology Institute, National University of Singapore, Singapore; and <sup>3</sup>Bioinformatics Institute, A\*STAR, Singapore

**ABSTRACT** Cyclic 3'5' adenosine monophosphate (cAMP)-dependent-protein kinase (PKA) signaling is a fundamental regulatory pathway for mediating cellular responses to hormonal stimuli. The pathway is activated by high-affinity association of cAMP with the regulatory subunit of PKA and signal termination is achieved upon cAMP dissociation from PKA. Although steps in the activation phase are well understood, little is known on how signal termination/resetting occurs. Due to the high affinity of cAMP to PKA ( $K_D \sim$  low nM), bound cAMP does not readily dissociate from PKA, thus begging the question of how tightly bound cAMP is released from PKA to reset its signaling state to respond to subsequent stimuli. It has been recently shown that phosphodiesterases (PDEs) can catalyze dissociation of bound cAMP and thereby play an active role in cAMP signal desensitization/termination. This is achieved through direct interactions with the regulatory subunit of PKA, thereby facilitating cAMP dissociation and hydrolysis. In this study, we have mapped direct interactions between a specific cyclic nucleotide phosphodiesterase (PDE8A) and a PKA regulatory subunit (RIα isoform) in mammalian cAMP signaling, by a combination of amide hydrogen/deuterium exchange mass spectrometry, peptide array, and computational docking. The interaction interface of the PDE8A:RIα complex, probed by peptide array and hydrogen/deuterium exchange mass spectrometry, brings together regions spanning the phosphodiesterase active site and cAMP-binding sites of RIα. Computational docking combined with amide hydrogen/deuterium exchange mass spectrometry provided a model for parallel dissociation of bound cAMP from the two tandem cAMP-binding domains of RIα. Active site coupling suggests a role for substrate channeling in the PDE-dependent dissociation and hydrolysis of cAMP bound to PKA. This is the first instance, to our knowledge, of PDEs directly interacting with a cAMP-receptor protein in a mammalian system, and highlights an entirely new class of binding partners for RIα. This study also highlights applications of structural mass spectrometry combined with computational docking for mapping dynamics in transient signaling protein complexes. Together, these results present a novel and critical role for phosphodiesterases in moderating local concentrations of cAMP in microdomains and signal resetting.

## INTRODUCTION

Cyclic 3'5' adenosine monophosphate (cAMP) is an important second messenger that is involved in relaying hormonal stimulation of membrane-bound G-protein-coupled receptors inside eukaryotic cells (1). cAMP levels are controlled both by G-protein-coupled-receptor-mediated activation of adenylyl cyclases, which synthesize cAMP from ATP (2), and cyclic nucleotide phosphodiesterases (PDEs), which catalyze hydrolysis of cAMP to 5'AMP (3). Even though cAMP is synthesized by adenylyl cyclases that are predominantly at the plasma membrane, it does not diffuse uniformly throughout the cell and instead exists in pools or microdomains (3–5). This has been attributed to diverse PDEs that function to limit cAMP diffusion. PDEs constitute a superfamily of enzymes with 11 families in mammals, consisting of cyclic 3'5' guanosine monophosphate (cGMP)-specific, cAMP-specific, and dual specific types. Of the cAMP PDEs, the PDE4 family has been most extensively characterized both in its enzy-

mology and in its interactions with other proteins or lipids to form large signaling complexes (6–10). Numerous studies have also shown unique targeting modes of diverse PDEs to distinct microdomains (11–13). An important basis proposed to account for the limited cAMP diffusion is via channeling of cAMP from cyclases to PDEs through the cAMP receptors in large macromolecular complexes (14).

cAMP binds to a diverse array of target proteins including protein kinase A (PKA), guanine exchange factor protein, cAMP-regulated bacterial transcription factors, and cyclic nucleotide-gated ion channels. The common feature in all of these diverse receptors is a highly conserved cAMP-binding domain (CNB), with a distinctive architecture and recognizable sequence of invariant residues critical for cAMP binding (15).

PKA is one of the most important targets for cAMP in eukaryotes (16) where the signaling cycle can be divided into activation and termination phases (Fig. 1). The regulatory (R) subunits of PKA exist as dimers, with each monomer containing a tandem array of CNB domains (referred to as CNB-A and CNB-B). Of all the CNB domain-containing proteins,

Submitted March 14, 2014, and accepted for publication July 15, 2014.

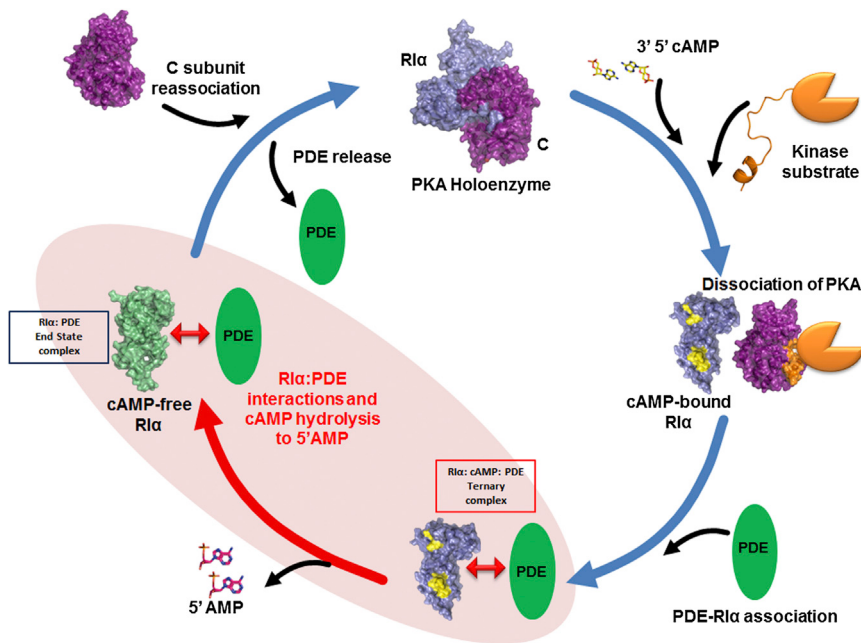
\*Correspondence: dbsgsa@nus.edu.sg

Editor: H. Wiley.

© 2014 by the Biophysical Society  
0006-3495/14/09/1426/15 \$2.00

<http://dx.doi.org/10.1016/j.bpj.2014.07.050>





(PDB:1RGS)), and RI $\alpha$ (91–379):C complex (PDB:2QCS). Only the monomeric deletion fragment of RI $\alpha$  (91–379) bound to PKA C-subunit (PDB:2QCS).

PKA R-subunits are unique in containing two tandem homologous CNB domains, whereby cooperative binding of cAMP to the two CNB domains initiates the activation phase. This is achieved through cAMP-dependent dissociation of the R-subunit from the catalytic (C) kinase core of PKA, leading to enhanced phosphorylation of numerous PKA cellular substrates (16). PKA has been the focus of extensive biochemical and structural studies and these have provided valuable snapshots of the stable endpoint conformations of inactive PKA holoenzyme and free active kinase (C-subunit) and cAMP-bound R-subunit (16–21). The molecular basis for cAMP action has been derived from dynamics studies by nuclear magnetic resonance (17,22–28) and hydrogen/deuterium exchange mass spectrometry (HDXMS) (29–31), aided by phosphorothioate analogs of cAMP (32,33). These studies have shown that the CNB domains in the R-subunit of PKA populate a continuum of conformations in solution wherein C-subunit and cAMP shift the equilibrium in separate directions to favor distinct endpoint conformations (33). This mode of action of cAMP is consistent with the conformational-selection model for ligand-mediated allosteric (34,35). Furthermore, dynamics have revealed that the two cAMP-binding sites are coupled, where cAMP binding to CNB-B leads to enhanced dynamics in CNB-A, when the binding pocket is disrupted by a point mutation. This provides an explanation for positive cooperativity in cAMP action (36). Together, these studies underscore how cAMP-induced changes in dynamics in PKA are critical for its function. All of these studies have focused entirely on the activation phase whereas the termination phase is poorly understood.

**FIGURE 1** Role of PDEs in signal termination of PKA-mediated cAMP pathway: The cAMP-PKA signaling pathway can be divided into Activation and Termination phases. Activation phase: In the presence of cAMP (yellow) and a kinase substrate (orange), the inactive PKA holoenzyme dissociates to yield the cAMP-bound PKA R-subunit (blue) and the active PKA C-subunit (purple). Termination phase: The role of PDEs in cAMP signal termination was demonstrated with the PDE, RegA (38,40). PDEs (green) mediate direct interactions with PKA R-subunit to hydrolyze cAMP bound to both CNB domains of PKAR. The resulting cAMP-free (apo) PKAR (green) is primed for reassociation with PKA C-subunit to form the inactive PKA holoenzyme. How PDEs interact with the R-subunit (RI $\alpha$  isoform) and catalyze hydrolysis of cAMP bound to the R-subunit to 5'AMP is unknown and a focus of this study (highlighted in red). We hypothesize that PDEs bind cAMP-bound RI $\alpha$  more tightly (ternary complex) than cAMP-free RI $\alpha$  (end-state complex). Space-filling models based on coordinates of structures of the different proteins are indicated. C-subunit (PDB:1ATP), R-subunit (cAMP-bound PKA RI $\alpha$ (113–379)

How the cAMP:PKA signaling system resets itself by regenerating inactive PKA holoenzyme can be defined as the resetting/termination phase. cAMP binds the PKA R-subunit with strong affinity (~2–10 nM) (37). How this tightly bound cAMP dissociates from its target R-subunit to allow for completion of the cAMP signaling cycle is an important mystery in cAMP signaling and is essential for signal termination. cAMP dissociation is critical to allow reassociation of PKA R-subunit with the C-subunit and resetting of the system through formation of the inactive PKA holoenzyme. A role for PDEs in termination by catalyzing hydrolysis of bound cAMP has come from recent studies with a cAMP PDE from *Dictyostelium discoideum*, RegA (38). *D. discoideum* represents an important model for cAMP signal termination because it lacks the complexity of isoforms in PKA and PDEs (39).

In this simpler system, the cAMP PDE RegA is capable of mediating dissociation and hydrolysis of cAMP bound to a PKA R-subunit through direct interactions (40) (Fig. 1). This is a critical step inasmuch as cAMP remains tightly bound to the R-subunit and shows negligible dissociation rates (41,42) in the absence of the C-subunit. The R-subunits thereby function to buffer intracellular cAMP and this is hydrolyzed through direct interactions with PDEs. This hydrolysis of bound cAMP is necessary for the R-subunit (RI $\alpha$  isoform) to reassociate with the C-subunit and reset the system through formation of the PKA holoenzyme (38). Indirect interactions of PDEs with PKA have been identified through the action of A-kinase anchoring proteins (AKAP) targeting proteins, which have been shown to localize PDEs and PKA (43–46). A direct role for PDEs in cAMP signal termination

was first hypothesized and tested with the PDE RegA (38,40). However, the nature of direct PDE-RI $\alpha$  interactions is completely unknown. Furthermore, no such interactions have been reported in mammalian cAMP signaling, whose complexity arises from myriad types/isoforms/splice variants of PDEs (3) and PKA.

In this study, we report a mammalian PDE:PKA RI $\alpha$  complex through an integrated approach combining structural mass spectrometry and fluorescence spectroscopy with computational methods. Although localization of PDEs with PKA R-subunits have been observed with specific classes of AKAPs (43), we describe, for the first time to our knowledge, AKAP-independent interactions between PKA and PDEs in a mammalian system. We also describe a mechanism for PDE-mediated dissociation of cAMP from the two binding sites on the R-subunit. The binding interface residues on RegA, mapped by HDXMS, were used to computationally identify PDE8 as a cAMP:PDE interacting partner; this was further validated by cAMP dissociation assays. A combination of HDXMS and computational docking was then used to map and model the PDE8:RI $\alpha$  interface. The power of computational docking has been greatly improved by combination with HDXMS, which provides experimental filters for narrowing the solutions for protein interfaces. This methodology has previously been used for mapping protein-protein interactions (47,48) and protein:DNA interactions (49). The PKA R-subunit is highly modular and is composed of an N-terminal dimerization domain, a pseudosubstrate site and two tandem CNB domains (18). The CNB domains are capable of functioning as high-affinity binders of both cAMP and the C-subunit in the absence of the dimerization domain. This has made it possible to use monomeric deletion mutant constructs of the pseudosubstrate region with CNB-A alone (residues 91–244) or as a construct spanning both CNB domains A and B together with the pseudosubstrate region (residues 75–379) for detailed mapping of PDE-R-subunit interactions. These are referred to as RI $\alpha_A$  and RI $\alpha_{AB}$ , respectively. Of the two PDE8 isoforms, we have used full-length PDE8A in this study or a deletion mutant spanning its catalytic domain (residues 472–829), henceforth referred to as PDE8A<sub>C</sub>.

Our results provide a minimal model to describe how a phosphodiesterase, PDE8, catalyzes hydrolysis of cAMP tightly bound to RI $\alpha$ . These results also provide a basis for how PDE-cAMP-receptors might form extended macromolecular complexes functioning as regulatory barriers for cAMP diffusion. PDEs we believe, are thus an entirely new class of RI $\alpha$ -interacting partner proteins involved in a novel mechanism for cAMP signal termination.

## EXPERIMENTAL PROCEDURES

### Materials

Unless otherwise mentioned, all reagents were from Sigma Aldrich (St. Louis, MO). BL21 (DE3) *Escherichia coli* strains were from Novagen

(Madison, WI). Glutathione Sepharose 4B and NHS-activated Sepharose 4 Fast Flow were obtained from GE Life Sciences (Chicago, IL). 8-AEA-cAMP was from Biolog Life Science Institute (Bremen, Germany); TFA, protein sequence analysis grade, was from Fluka BioChemika (Buchs, Switzerland); and the Poroszyme-immobilized pepsin cartridge was from Applied Biosystems (Foster City, CA). Purified recombinant GST-tagged PDE2A (catalog No. 60020), PDE5A (catalog No. 60050), PDE8A (catalog No. 60080), and PDE9A (catalog No. 60090) were purchased from BPS Bioscience (San Diego, CA). Recombinant GST-tagged PDE8A (1 mg/mL) was also obtained from Signal Chem (Richmond, British Columbia, Canada) for HDXMS experiments.

### Subcloning of PDE8A<sub>C</sub> and full-length RI $\alpha$ into pETDuet-1 vector

Oligonucleotide primers for PDE8A catalytic domain spanning residues 472–829, were designed using codon-optimized Human PDE8A1 synthetic gene as a template (DNA 2.0; Menlo Park, CA). The DNA fragments were amplified by polymerase-chain reaction and subcloned using *Bam*H and *Nor*I restriction enzymes into a multiple cloning site 1 (MCS1) of the pETDuet-1 vector containing a hexahistidine tag, N-terminal to the protein sequence. Full-length RI $\alpha$  was cloned into a multiple cloning site 2 (MCS2) of the pETDuet-1 vector using the *Nde*I and *Kpn*I restriction enzymes.

### Protein expression and purification

PDE8A<sub>C</sub> has been expressed in *E. coli* but is insoluble and present in inclusion bodies (50). We hypothesized that coexpression of full-length RI $\alpha$  with PDE8A<sub>C</sub> in *E. coli* BL21 (DE3) cells might aid solubility of PDE8A<sub>C</sub>. Although some of the PDE8A<sub>C</sub> was found to be soluble, most of it was still present in inclusion bodies. To improve yields of soluble PDE8A<sub>C</sub>, refolding of inclusion bodies with denaturants was carried out. Thus, the pellet with insoluble PDE8A<sub>C</sub> was denatured by 6 M guanidinium hydrochloride and the solubilized PDE8A<sub>C</sub> was purified by affinity chromatography using Cobalt affinity His-Tag resin (Clontech Laboratories, Mountain View, CA). PDE8A<sub>C</sub> was refolded by a previously described protocol in Yan et al. (50), with the only modification being that the Hexahistidine tag was not removed by thrombin cleavage. Refolded PDE8A<sub>C</sub> showed the same activity as reported in Yan et al. (50).

cAMP affinity chromatography resin for R-subunit purification was synthesized by coupling 8-AEA-cAMP to the NHS-activated Sepharose 4 Fast-Flow beads according to manufacturer specifications (GE Life Sciences, Singapore) (51). Both cAMP-bound and cAMP-free RI $\alpha_A$  were expressed and purified as described previously in Anand et al. (52). cAMP-bound RI $\alpha_{AB}$  was expressed and purified by cAMP affinity chromatography resin similar to RI $\alpha_A$ . The cAMP-free RI $\alpha_{AB}$  was prepared by the dissociation of cAMP by urea stripping and refolding (53). RegA (385–780) (RegA<sub>C</sub>) was expressed as a GST fusion protein in *E. coli* BL21\*(DE3). The protein was purified using glutathione Sepharose 4B (GE Life Sciences) according to manufacturer specifications followed by size exclusion-gel filtration chromatography on an AKTA system (GE Life Sciences) (38).

### Fluorescence polarization assay for cAMP dissociation

To determine whether all PDEs were capable of dissociating bound cAMP from RI $\alpha$ , we carried out a fluorescence polarization (FP) assay using 8-Fluo-cAMP (8-(2-[fluoresceinyl]aminoethylthio)adenosine- 3',5'- cyclic monophosphate) saturated RI $\alpha_A$  as described in Moorthy et al. (38) with PDEs 2A,5A, 8A, and 9A. A Synergy 4 Multi-Detection microplate reader (Biotek, Winooski, VT) was used in FP mode for the plate reader assays. The excitation and emission wavelengths used were 485 and 528 nm, respectively, with a bandwidth of 20 nm with an instrument G-factor of 0.87. Ninety-six-well black plates

were from Greiner Bio-One (Frickenhausen, Germany). The FP signals for 0.12  $\mu\text{M}$  of 8-Fluo-cAMP-bound RI $\alpha_A$  in buffer A (20 mM Tris-HCl, pH 7.5, 50 mM NaCl, 10 mM MgCl<sub>2</sub>, and 5 mM BME) were monitored in the presence of a 10-fold molar excess of PDE and were repeated with equimolar PDE8A. FP measurements were taken at time intervals of 2 min up to 45 min. In all samples, 0.5 mM cAMP/10  $\mu\text{M}$  cAMP/cGMP was added at 18 min. When excess PDE was used to monitor FP, 0.5 mM cAMP was used to saturate the reaction whereas 10  $\mu\text{M}$  of cAMP/cGMP was used when lower concentrations of PDE8A were tested subsequently. Data from early time points (0–18 min) were fit to a one-phase exponential decay equation using the software GRAPH-PAD PRISM, Ver. 5 (GraphPad, San Diego, CA).

## Amide hydrogen/deuterium exchange mass spectrometry

To carry out amide hydrogen/deuterium exchange mass spectrometry (HDXMS) experiments of the GST-RegA<sub>C</sub>:RI $\alpha_A$  complex, 50  $\mu\text{L}$  of 20  $\mu\text{M}$  GST-RegA<sub>C</sub> and 60  $\mu\text{M}$  cAMP-free RI $\alpha_A$  (1:3 molar ratio) were incubated at room temperature for 30 min.

HDXMS experiments with the full-length PDE8A1:RI $\alpha_A$  complex were carried out maintaining sample concentration at 6  $\mu\text{M}$  of PDE8A1 and 42  $\mu\text{M}$  of cAMP-free RI $\alpha_A$  (1:7 molar ratio) in a total reaction volume of 4  $\mu\text{L}$  for each HDXMS experiment.

HDXMS experiments of the PDE8A<sub>C</sub>:RI $\alpha_{AB}$  complex were carried out in two ways: 1), to maintain saturating amounts of RI $\alpha_{AB}$  and maintain all available PDE8A<sub>C</sub> in complex form, 30  $\mu\text{M}$  of PDE8A<sub>C</sub> was incubated with 90  $\mu\text{M}$  cAMP-bound RI $\alpha_{AB}$  (1:3 molar ratio) for 1 h on ice; and 2), for the inverse experiment, where saturating amounts of PDE8A<sub>C</sub> are maintained so all available RI $\alpha_{AB}$  is in complex form, 30  $\mu\text{M}$  of cAMP-bound RI $\alpha_{AB}$  was incubated with 100  $\mu\text{M}$  of PDE8A<sub>C</sub> (1:3.3 molar ratio) for 1 h on ice. Incubating cAMP-bound RI $\alpha_{AB}$  with PDE8A<sub>C</sub> was carried out to obtain the end-state complex of cAMP-free RI $\alpha_{AB}$  bound to PDE8A<sub>C</sub>. An incubation time of 1 h was determined to be optimal, from HDXMS-based real-time reaction monitoring experiments, for complete PDE8A<sub>C</sub>-mediated cAMP dissociation from RI $\alpha_{AB}$ . These experiments showed that all available cAMP bound to RI $\alpha_{AB}$  was dissociated and hydrolyzed within 30 min by PDE8A<sub>C</sub> action, resulting in cAMP-free RI $\alpha_{AB}$  bound to PDE8A<sub>C</sub>. This was observed even when RI $\alpha_{AB}$  was at 3 $\times$  higher molar concentration to PDE8A<sub>C</sub> (S. Krishnamurthy, N. K. Tulsian, and G. S. Anand, unpublished results). Control HDXMS experiments with cAMP-free RI $\alpha_{AB}$  were carried out with urea-stripped and refolded RI $\alpha_{AB}$ .

All samples were allowed to equilibrate to room temperature before deuterium exchange experiments. Deuterium exchange was carried out by diluting the samples in storage buffer (20 mM Tris-HCl, pH 7.5, 50 mM NaCl, 10 mM MgCl<sub>2</sub>, and 5 mM BME) 15 $\times$  for RegA:PKA R-subunit complex in D<sub>2</sub>O (99.90%), resulting in a final concentration of 93.3% deuterated buffer. For PDE8A:RI $\alpha_{AB}$  complexes (both full-length PDE8A and PDE8A<sub>C</sub>), samples were diluted 10 $\times$  in storage buffer, resulting in a final concentration of 90% deuterated buffer.

Exchange was carried out at 20°C for various labeling times (0.5, 1, 2, 5, and 10 min). For initial experiments with full-length PDE8A, only a single labeling time of 2 min was carried out. The exchange reaction was quenched by addition of prechilled 0.1% TFA to obtain a final pH<sub>read</sub> of 2.5. Fifty microliters of the quenched sample was then injected on to a chilled nano-UPLC sample manager (Waters, Milford, MA) as previously described in Wales et al. (54). The sample was washed through a 2.1  $\times$  30-mm immobilized pepsin column (Porozyme; ABI, Foster City, CA) using 100  $\mu\text{L}/\text{min}$  0.05% formic acid in water. The digest peptides were trapped with a 2.1  $\times$  5 mm C18 trap (ACQUITY BEH C18 VanGuard Pre-column, 1.7  $\mu\text{m}$ ; Waters). Peptides were eluted using an 8–40% gradient of acetonitrile in 0.1% formic acid at 40  $\mu\text{L}/\text{min}$ , supplied by a nanoACQUITY Binary Solvent Manager (Waters), into a reverse phase column (ACQUITY UPLC BEH C18 Column, 1.0  $\times$  100 mm, 1.7  $\mu\text{m}$ ; Waters) for resolution. Peptides were detected and mass-measured on a SYNAPT HDMS mass spectrometer (Waters) acquiring in MS<sup>E</sup> mode (55,56).

Peptides were identified from MS<sup>E</sup> data of undeuterated samples using the PROTEINLYNX GLOBAL SERVER (PLGS 2.4; Waters) (57,58). Identifications were only considered if they appeared at least twice out of three replicate runs and had a minimum of four digest fragment ions. These identifications were mapped onto subsequent deuteration experiments using prototype custom software (DYNAMX Ver. 2.0; Waters). Data on each individual peptide at every time point was extracted and analyzed using this software. Instrument calibration was carried out as described in Anand et al. (32) and Moorthy et al. (36). Reported values for all HDXMS experiments are the average of at least two independent deuterium exchange experiments.

## Docking

The model of PKA RI $\alpha_{AB}$  bound to PDE8A<sub>C</sub> was generated using the HADDOCK web server (59). The available crystal structures of dimeric PDE8A<sub>C</sub> (PDB:3ECN) and the cAMP-bound conformation of RI $\alpha$  (PDB:1RGS) were considered as starting structures for the docking. Because the linker between the two cAMP domains of RI $\alpha$  is highly flexible, leading to potentially large conformational changes upon binding PDE8, RI $\alpha$  was split into two CNB domain fragments, namely RI $\alpha$ \_CNB-A (residues 113–235) and RI $\alpha$ \_CNB-B (residues 241–379) and docked independently. The active residues that drive the docking calculations were selected based on regions showing decreased deuterium exchange upon complexation with PDE8. Because this region outlined by the experiment was large and includes residues that are buried in the static crystal structure, we only selected a subset of residues that were solvent-exposed as the input for docking. The residues around the active residues were considered passive (the default option). The C- and N-termini were kept uncharged inasmuch as they were not the actual termini. The residues 230–235 in RI $\alpha$ \_CNB-A and 241–250 in RI $\alpha$ \_CNB-B were treated as fully flexible. For each run, 1000 structures, in total, were calculated by rigid-body minimization of the docking score. Semiflexible simulated annealing followed by refinement in explicit water was performed for the best 200 solutions based on the HADDOCK score. The calculated models were clustered using a 7.5 Å interface root-mean-square deviation cutoff.

The following residues were defined as ambiguous interaction restraints to drive the docking:

### PDE8A residues

526, 527, 529, 530, 531, 532, 609, 610, 611, 621, 622, 651, 652, 653, 681, 682, 683, 686, 687, 690, 691, 693, 694, 696, 698, 699, 700, 702, 703, 706, 756, 759, 760, 761, 762, and 763.

### RI $\alpha$ (CNB-A) residues

128, 131, 132, 133, 134, 171, 177, 178, 179, 189, 191, 194, 196, 197, 199, 200, 201, 204, 205, 206, 207, 208, 210, 216, 217, and 218.

### RI $\alpha$ (CNB-B) residues

268, 269, 270, 271, 272, 273, 274, 275, 276, 277, 278, 322, 323, 324, 325, 328, 329, 330, 331, 332, 333, 334, 335, 336, 354, 355, 356, 358, 359, 361, 362, and 363.

## Selection of the docked pose

The binding models of the CNB-A and CNB-B to the PDE8A<sub>C</sub> dimer from the docked poses of two independent runs were picked based on the following criteria:

1. The quality of RI $\alpha$  contacts with the PDE8A<sub>C</sub> (using the native HADDOCK score),
2. The accessibility of the RI $\alpha$ -bound cAMP to the catalytic site of the PDE8A<sub>C</sub>, and

3. Whether the distance and orientation of the two independently docked domains was consistent with the fact that the two are connected by the RI $\alpha$  linker  $\alpha$ :C-helix in vivo.

Criterion 2 was quantitated in an ad hoc way by counting the number of peptide atoms inside the sphere that can be inscribed between the centers of the cAMP-binding pockets in PDE and RI $\alpha$ . Namely, if our model is correct, we expect that the cAMP-binding pockets in the two proteins should be mutually accessible, allowing the transfer of the substrate between the two. Thus, we looked for a configuration of the complex in which as few peptide atoms as possible appear in the space between the two pockets. Criterion 3 was tested by manually modeling the central helix into the model of the complex.

## RESULTS

### The RI $\alpha$ CNB:A-RegAc interface by HDXMS encompasses the PDE catalytic active site

We previously showed that the catalytic domain of *D. discoideum* RegA (RegA<sub>C</sub>) was capable of interacting with the mammalian PKA R-subunit (RI $\alpha$ ) to dissociate bound cAMP and hydrolyze it to 5'AMP (38). Because PKA R-sub-

units have two CNB domains, initial experiments used the single domain CNB-A construct and mapped the binding site for RegA<sub>C</sub> (38), which overlapped with the cAMP-binding site (40). Here we mapped the complementary interaction surface on RegA<sub>C</sub> by a combination of peptide array and HDXMS (see Fig. S1 and Fig. S2 in the Supporting Material). The results enabled a detailed map of the interface that encompassed the PDE active site when modeled onto the structure of a close cAMP PDE homolog of RegA, PDE8A (PDB:3ECM) using the software SWISS-MODELER (Fig. 2, A–C, and see the Supporting Material) (60,61).

### PDE-RI $\alpha$ interaction interface shows broad conservation across the PDE superfamily

The binding site for RegA on PKA RI $\alpha$  identified by HDXMS and peptide array (Fig. 2, D and E) spanned the RegA catalytic site, which is highly conserved across all PDEs. This suggested PDE:PKA RI $\alpha$  complexes might be conserved in mammalian cAMP signaling wherein one or

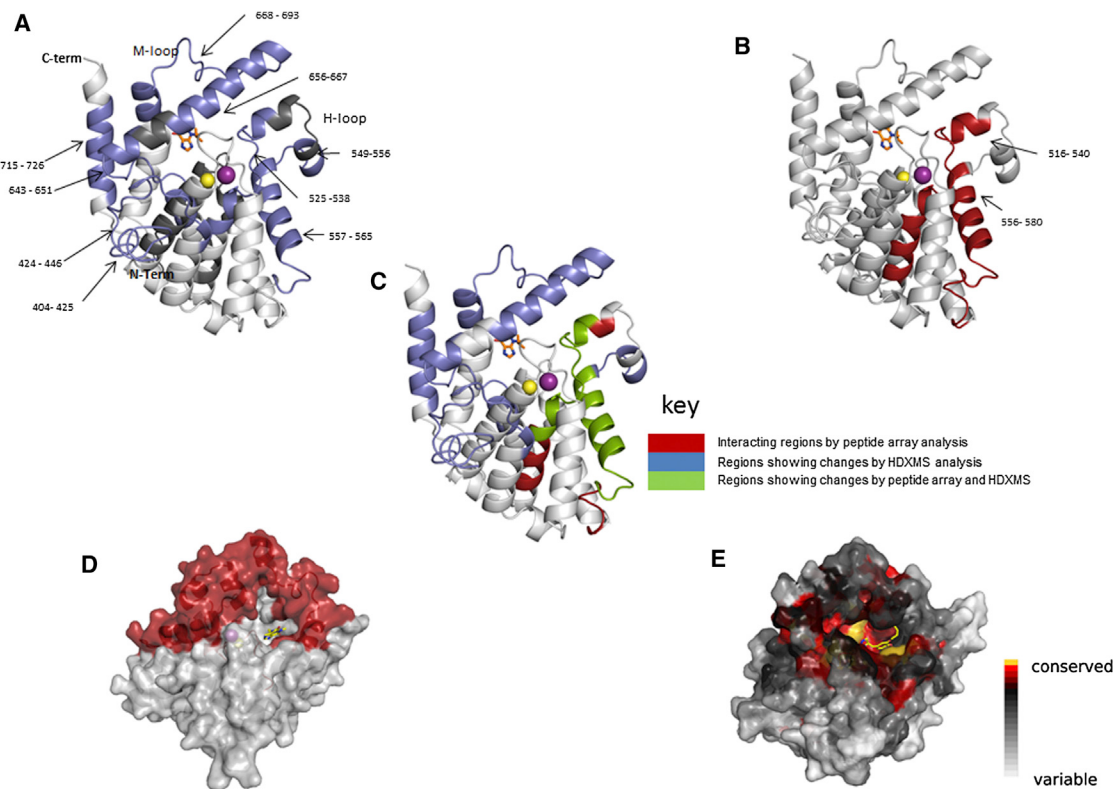


**FIGURE 2** Summary of peptide array analysis and HDXMS of RI $\alpha$ :RegAc interactions mapped onto the structure of PDE8A. (A) Results from HDXMS for the catalytic domain of RegA mapped onto the homology-modeled PDE structure of the closest cAMP PDE homolog of RegA, PDE8 (PDB:3ECN) using SWISS-MODELER. (Blue) Peptide fragments showing decreased exchange (after 10 min deuterium exchange) in the presence of RI $\alpha$ . (White) Regions showing no difference; (dark gray) regions with no pepsin-digest fragment coverage. (B) Results from peptide array analysis for RegA<sub>C</sub> mapped onto the homology-modeled PDE structure of PDE8A (PDB:3ECN). (Red) Peptides showing direct interactions with RI $\alpha$ . (C) Composite of HDXMS and peptide array results mapped onto the structure of homology-modeled PDE8. (Blue regions) Decreased exchange; (red regions) peptide array fragments; and (green regions) intersection sites. In addition to Zn<sup>2+</sup> and Mg<sup>2+</sup>, the nonspecific PDE inhibitor, IBMX (3-isobutyl-1-methylxanthine) is shown in panels B and C (stick representation). (D) Results from HDXMS of RegA<sub>C</sub>:RI $\alpha$  interactions are mapped (red) onto the surface representation of the modeled RegA structure. The inhibitor IBMX is shown in stick representation (yellow). (E) Evolutionary trace analysis of RegA:RI $\alpha$  interaction interface mapped onto the structure of the cGMP phosphodiesterase PDE9 (PDB:2HD1).

more mammalian PDE homologs of RegA could mediate functional interactions with PKA R-subunits including RI $\alpha$ . To examine this further, we carried out a comprehensive primary sequence analysis based on sequence conservation and exon-intron structure, to identify putative mammalian homologs of RegA from within the PDE superfamily (see Fig. S3 and Fig. S4). These analyses revealed a strong sequence conservation in RI $\alpha$  interaction regions, which also overlapped with the highly conserved phosphodiesterase active sites. If we narrowed down the sequence homology to just the catalytic domains alone, we found to our surprise the closest mammalian PDE homolog to be a cGMP-specific PDE, PDE9. This was intriguing as it highlighted a possible route for cross-talk between cGMP and cAMP signaling. The next-nearest homologous catalytic domain was the cAMP PDE, PDE8. Interestingly, the domain organization of PDE8A shows parallels with RegA, in containing a putative N-terminal response regulator domain (receiver domain) (39,62).

### Rapid screening of PDE-RI $\alpha$ interactions by fluorescence polarization spectroscopy

To test the potential broad specificity of PDE interactions with RI $\alpha$ , we used Fluorescence polarization spectroscopy (FP) with 8-fluo-cAMP (8-(2-[fluoresceinyl]aminoethylthio)adenosine-3',5'-cyclic monophosphate) as a rapid screen for identifying potential PDEs that are capable of dissociating cAMP bound to the PKA R-subunit. We chose four full-length PDEs (PDE9A, PDE8A, PDE2A, and PDE5A) to test for dissociation of cAMP bound to the CNB-A domain of RI $\alpha_A$ . To broaden the search for possible mammalian homologs of RegA, we also included two classes of cyclic nucleotide-binding GAF-domain regulated PDEs, PDE5A (cGMP-specific) and PDE2A (cAMP/cGMP dual specificity) for testing interactions with RI $\alpha$ . FP assays with 8-fluo-cAMP -labeled RI $\alpha_A$  were carried out as described in Moorthy et al. (38). 8-fluo-cAMP is resistant to PDE hydrolysis and therefore offered an opportunity for direct monitoring of cAMP dissociation from RI $\alpha$  (63). No intrinsic dissociation of 8-fluo-cAMP was observable from CNB-A of RI $\alpha$  in the absence of either excess cAMP or excess PDE. This is a consequence of a slow kinetic off-rate for cAMP from the R-subunit or fast reassociation rate of released cAMP, and was used as a basis for testing the ability of PDEs to dissociate cAMP bound to CNB-A in RI $\alpha_A$ .

In the presence of a 10 $\times$  molar excess of full-length PDEs, small increases in FP values were observable with time in the presence of PDEs 5A and 8A. This can be attributed to the ability of PDEs to bind 8-fluo-cAMP despite being incapable of readily hydrolyzing it (63). Even though equivalent analogs resulting from substitutions at the 8' position of the adenine ring such as 8-Br-cAMP confer resistance to PDE hydrolysis, they nevertheless are capable of binding and functioning as

competitive inhibitors of PDEs. Addition of PDE2A resulted in a steady increase in fluorescence polarization with time (Fig. 3 A). This increase in FP is consistent with 8-fluo-cAMP functioning as a cAMP analog and binding the GAF domain of PDE2. Regardless of how 8-fluo-cAMP might interact with PDEs, the increase in FP upon addition of PDEs 2A, 5A, and 8A could only occur upon its dissociation from RI $\alpha_A$ .

To measure the ability of cAMP to competitively displace 8-fluo-cAMP from RI $\alpha_A$ , a vast excess of cAMP (0.5 mM) was added and the FP signal monitored. The addition of excess cAMP after 18 min showed important differences between the cGMP-specific and cAMP-specific PDEs. This time point was chosen for addition of cAMP based on our previous observations, where addition of RegA PDE resulted in a complete drop in FP within 10 min (38). cAMP addition was carried out at this time point (18 min) to allow possible PDE-mediated dissociation to be fully completed before introducing excess cyclic nucleotides in the reaction. Samples containing PDEs 5A and 9A

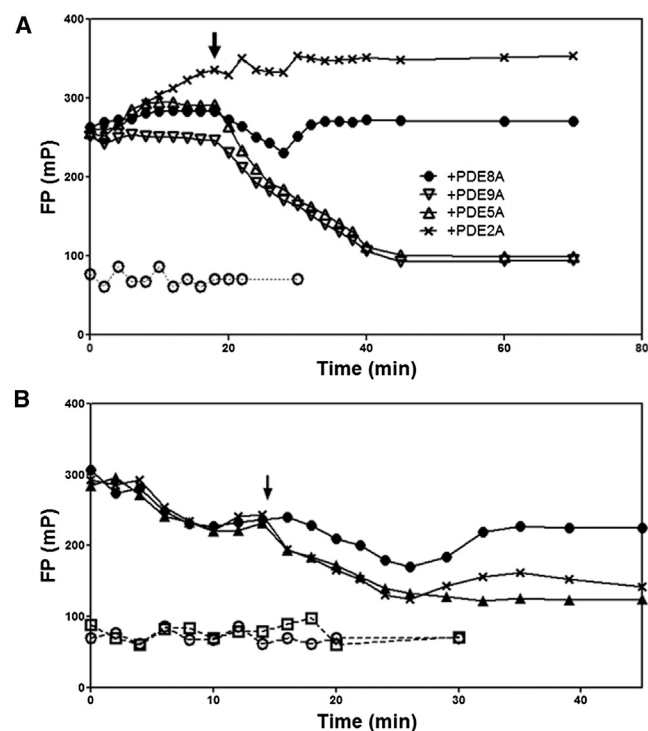


**FIGURE 3** PDE8A interacts with RI $\alpha$  and blocks cAMP reassociation. (A) Dissociation of 8-fluo-cAMP from RI $\alpha_A$ (0.12  $\mu$ M) was monitored by measuring the fluorescence polarization (FP) change in the presence of a molar excess (1.2  $\mu$ M) of the following phosphodiesterases (×) PDE2A, (●) PDE8A, ( $\Delta$ ) PDE5A, and ( $\nabla$ ) PDE9A. Interpolated FP values are plotted versus time; (arrow) addition of cAMP (0.5 mM) after 18 min to all reactions. Baseline signal for 8-fluo-cAMP (0.12  $\mu$ M) (○). (B) Dissociation of 8-fluo-cAMP from RI $\alpha_A$ (0.12  $\mu$ M) was monitored by measuring the FP change in the presence of 0.13  $\mu$ M PDE8A (●) and IBMX-saturated PDE8A (×); (arrow) addition of cAMP (10  $\mu$ M) or cGMP (10  $\mu$ M) ( $\blacktriangle$ ) after 18 min of the reaction. Baseline signal for 8-fluo-cAMP (0.12  $\mu$ M) (○) and PDE8A (0.12  $\mu$ M) (□).

showed a steady drop in FP up to time  $t = 40$  min when it reached baseline, upon addition of cAMP. Because cAMP is hydrolyzed poorly by cGMP PDEs, all of the 8-fluo-cAMP bound to RI $\alpha$  is displaced by excess unhydrolyzed cAMP and this is reflected in the drop in FP.

The sample containing PDE8A showed a more gradual drop in FP upon addition of cAMP up to time  $t = 28$  min, after which it increased to a steady intensity at time  $t = 32$  min, equivalent to the signal at time  $t = 18$  min before the addition of cAMP. PDE8A rapidly hydrolyzes the excess cAMP added to 5'AMP and once the cAMP is depleted, 8-fluo-cAMP reassociates with PDE8A to increase the FP signal (Fig. 3 A). All the PDEs we tested, with the exception of PDE9A, were capable of interactions with RI $\alpha_A$  resulting in dissociation of cAMP. Although these results do not exclude PDEs 2A and 5A as potential RI $\alpha_A$  binders, we chose to explore these PDE8A:RI $\alpha_A$  interactions further, given its higher homology with RegA.

### PDE8A interacts with RI $\alpha$ and facilitates cAMP dissociation

We next carried out FP assays at lower concentrations of PDE8A ((0.13  $\mu$ M), 1:1 molar ratios). At these lower concentrations, we observed that PDE8A alone showed no changes in FP, suggesting that it did not bind 8-fluo-cAMP (Fig. 3 B). These conditions therefore allowed monitoring of cAMP dissociation by PDE8A. Our results showed that PDE8A promotes dissociation of 8-fluo-cAMP both in the presence and absence of the nonspecific PDE inhibitor IBMX (3-isobutyl-1-methyl xanthine). Upon addition of excess cAMP, a larger dip in the FP signal was observed for IBMX-bound PDE8A. This reflects slower cAMP hydrolysis in the presence of IBMX and consequently a lag in reassociation of released 8-fluo-cAMP to RI $\alpha$  (Fig. 3 B).

PDE assays showed that PDE8A was capable of hydrolyzing cAMP bound to RI $\alpha_A$  with cAMP-bound RI $\alpha_A$  as the sole substrate (see Fig. S5). This is consistent with previous results obtained with RegA (38). We then set out to examine the interactions of the catalytic domain of PDE8A with the CNB domains of PKA R-subunit in greater detail.

### Catalytic domain of PDE8A interacts with both cAMP-binding domains of RI $\alpha$

Having shown that PDE8A was capable of dissociating cAMP bound to RI $\alpha_A$ , we set out to map complexes of PDE8A with RI $\alpha_A$  and compare it with RegA:RI $\alpha_A$  complex. Full-length PDE8A was complexed with cAMP-free RI $\alpha_A$  and HDXMS was carried out on the complex, as described in the Experimental Procedures. Given that the locus of interactions between RI $\alpha_A$  and RegA was entirely within the RegA catalytic domain (38), deuterium exchange

analysis for PDE8A was restricted to the catalytic domain. Twenty-four peptides, total, were analyzed corresponding to a sequence coverage of 72% for the catalytic domain (residues 480–818). Four regions showed decreased deuterium exchange upon binding to RI $\alpha_A$  (see Fig. S6). The regions span residues 527–547 of H4 and H5, 619–648 of H10, 765–781 of the M-loop, and 685–706 on HE1 and HE2. Of these regions, three are proximal to the catalytic site whereas residues 685–706, represented by two contiguous peptides, are located on a helix loop helix motif (HE1 and HE2) unique to PDE8 (61).

For improved resolution of the PDE8-RI $\alpha$  interface, we then focused on the catalytic domain of PDE8A, PDE8A<sub>C</sub>. Size-exclusion chromatography of PDE8A<sub>C</sub> showed two peaks representing a dimer and monomer with a concentration-dependent elution of a majority of PDE8A<sub>C</sub> as a dimer (data not shown). Given that PDE8A and other PDEs exist as dimers in solution (3), we tested for how a PDE dimer (PDE8A<sub>C</sub>) might engage both CNB domains in RI $\alpha$ . We therefore set out to map interactions by HDXMS with an expanded monomeric RI $\alpha$  fragment containing both CNB domains (RI $\alpha_{AB}$ ) with dimeric PDE8Ac.

Sixty-nine peptides, total, were observed and analyzed by HDXMS, which corresponds to a coverage of 81% of the primary sequence of PDE8A<sub>C</sub>. On PDE8A<sub>C</sub>, regions spanning the conserved catalytic residues showed decreased exchange in the PDE8A<sub>C</sub>:RI $\alpha_{AB}$  complex (Figs. 4 and 5), and overlapped with the regions that showed decreased exchange in full-length PDE8A.

In the converse HDXMS experiment to map the interaction of PDE8A<sub>C</sub> onto the surface of RI $\alpha_{AB}$  in the RI $\alpha_{AB}$ :PDE8A<sub>C</sub> complex, 49 peptides were observed and quantified, corresponding to a coverage of 80% of the primary sequence of RI $\alpha_{AB}$ . The RI $\alpha_{AB}$ :PDE8A<sub>C</sub> complex was generated by incubating RI $\alpha_{AB}$  with a 3 $\times$  molar excess of PDE8A<sub>C</sub> for 1 h to ensure all the cAMP bound is fully dissociated from the complex. Interestingly, results for RI $\alpha_{AB}$  showed decreased exchange at both cAMP-binding sites (CNB-A and CNB-B) and across regions connecting these two domains (Figs. 6 and 7). Sites showing the greatest shifts in deuterium exchange upon complexation with PDE8A<sub>C</sub> thus were not only at the binding sites but also at flanking allosteric sites important for propagation of the effects of cAMP binding. Importantly, N-terminal regions of RI $\alpha_{AB}$  spanning the PKA pseudosubstrate site showed only minor changes in deuterium exchange upon complexation with PDE8A<sub>C</sub>. (See Table S1 and Table S2 in the Supporting Material summarizing deuterium exchange for all the peptides from PDE8A<sub>C</sub> and RI $\alpha_{AB}$ .)

The effects of cAMP binding on RI $\alpha_{AB}$  (Fig. 8 A, top panel) were different from the effects of PDE complexation (Fig. 6, bottom panel). This is summarized in Fig. 8 A (bottom panel). cAMP-binding results in large-magnitude decreases in deuterium exchange, which are primarily within the specific binding pockets in CNB-A and CNB-B. The

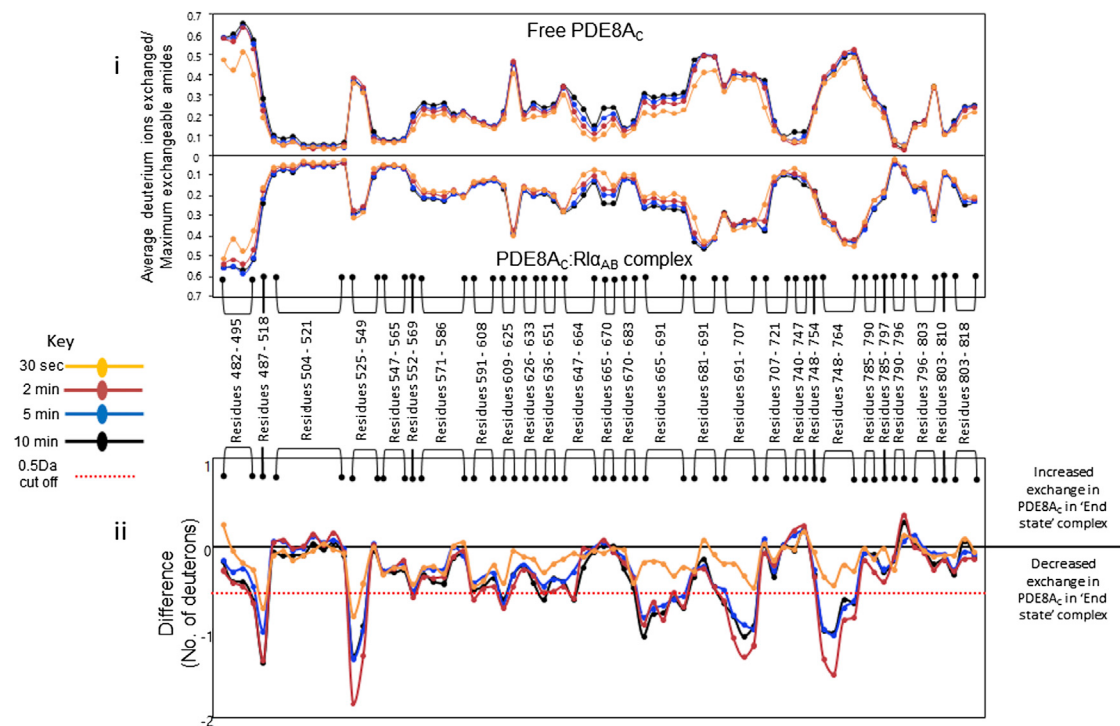


**FIGURE 4** Proteinwide overview of interaction of RI $\alpha_{AB}$  on PDE8A<sub>C</sub>. *(i)* Mirror plot representation for comparative analysis of HDXMS of free PDE8A<sub>C</sub> (catalytic domain) and in the presence of RI $\alpha_{AB}$ . The relative deuterium exchange (y axis) of each pepsin digest fragment is listed from the N- to C-terminus (x axis) of PDE8A<sub>C</sub>, with deuterium exchange times color-coded as per key. In this plot, relative deuterium exchange (y axis) of free PDE8A<sub>C</sub> (*upper half*) is compared with relative deuterium exchange of PDE8A<sub>C</sub> in complex with RI $\alpha_{AB}$  (*lower half*). *(Bottom panel)* Absolute difference in numbers of deuterons (inferred from difference in mass in Daltons (Da) (y axis) between the free and complexed state is plotted for each pepsin digest fragment listed from the N- to C-terminus (x axis) of PDE8A<sub>C</sub> for each deuterium exchange time point ( $t = 0.5, 2, 5, 10$  min) in a difference plot. Shifts in the positive scale represent increases in deuterium exchange and shifts in the negative scale represent decreases in deuterium exchange. A difference of 0.5 Da is considered significant (*dashed red line*). Plots were generated using the software DYNAMX (Ver. 2.0, Waters). Each point represents a pepsin digest fragment, and brackets group the overlapping fragment peptides.

PDE8A<sub>C</sub> complexation, on the other hand, shows smaller magnitude decreases in the cAMP-binding sites; however, it also shows proteinwide decreases in deuterium exchange (Fig. 8*B*) and specifically in the N-terminus and the interdomain  $\alpha$ :C helix.

#### Model of PDE8A-RI $\alpha$ interface by computational docking reveals both CNB domains of RI $\alpha_{AB}$ are in close proximity to PDE8A<sub>C</sub> catalytic site

Molecular docking was carried out to model the PDE8:PKA RI $\alpha$  interface based on the HDXMS results. Because size exclusion chromatography of PDE8A<sub>C</sub> indicated a majority of PDE8A<sub>C</sub> existed as a dimer in solution, and the PDE8 structure (PDB:3ECN) crystallized as a dimer, the dimeric structure of the catalytic domain of PDE8, was used for docking with monomeric RI $\alpha$ (113–379) ((PDB:1RGS)). Such a complex would show a stoichiometry of one PDE dimer interacting with one monomer of RI $\alpha$ (113–379).

RI $\alpha$  exists in two distinct conformations: 1), bound to PKA catalytic subunit (H-form), and 2), bound to cAMP (B-form) (33,64). We hypothesize that the B-form of

RI $\alpha$  must interact with PDEs (ternary complex) for hydrolysis of the tightly bound cAMP, leading to cAMP signal termination (Fig. 1). These can occur through a simultaneous interaction of the two cAMP-bound CNB-domains or via tandem binding of each cAMP-bound CNB domain to individual PDE units in the dimer. Because it is known that the two cAMP-binding domains in RI $\alpha$  are connected by a dynamic C-helix (36,65), we reasoned that the central helix undergoes dynamic rearrangements, making accommodation of both CNB domains binding simultaneously or in tandem equally plausible. Furthermore, mapping of PDE8:RI $\alpha$  interactions by HDXMS suggests that the PDE8-binding interface is symmetric, whereas differential exchange across the two CNB domains of RI $\alpha$  is nonuniform. These are suggestive of an asymmetric interaction surface across the individual CNB domains of RI $\alpha$ . To factor in dynamics of the interdomain linker (64,66), HADDOCK runs were set up in two different ways: The cAMP-bound conformation of RI $\alpha$  (PDB:1RGS chain B) was modeled as follows:

1. As one whole unit with a rigid helix linker, and
2. As two separate cAMP-binding domains sans the linker.

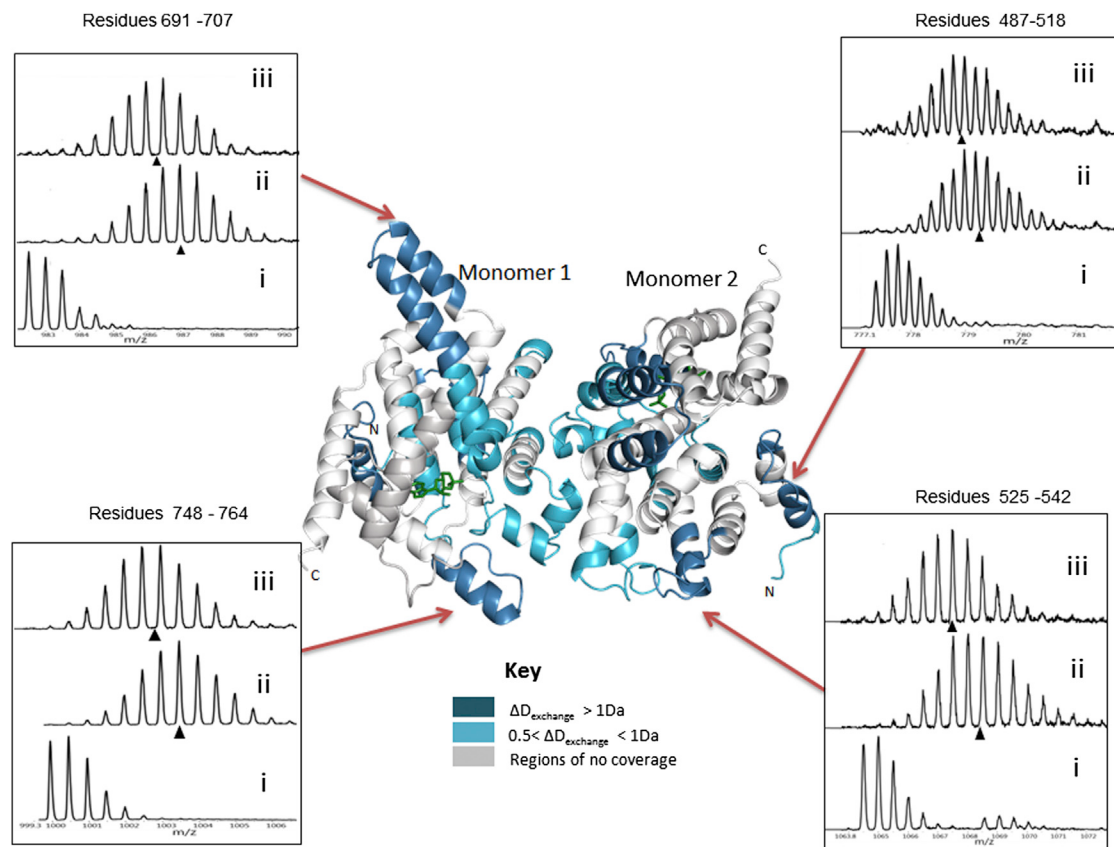


**FIGURE 5** Map of the interactions of RI $\alpha_{AB}$  on PDE8A $_C$ . Effects of RI $\alpha_{AB}$  interactions from HDXMS analysis mapped onto the dimeric structure of PDE8A $_C$  (PDB:3ECN); IBMX at the active site is in green. (*Shadings in blue*, as per key) Regions of PDE8A $_C$  showing significant decreases in deuterium exchange upon complex formation. Mass spectra of peptides showing significant changes upon RI $\alpha_{AB}$  complex formation (difference  $> 1 \text{ Da}$ ) are shown. The isotopic envelopes of pepsin fragment peptides of (i) undeuterated control of PDE8A $_C$ , (ii) free PDE8A $_C$  after 2 min deuteration, and (iii) PDE8A $_C$  in a complex with RI $\alpha_{AB}$  after 2 min deuteration are depicted. Centroids are indicated ( $\blacktriangle$ ).

In the latter runs, to circumvent the limitation of docking programs in modeling large conformational changes, each CNB domain was independently docked to mimic the freedom that a flexible linker would provide. It is well established that the solutions generated by HADDOCK are closer to native complexes if the docking is driven by restraints based on experimental data. In our case, these constraints were provided by results from HDXMS. The changes in deuterium exchange upon complexation in PDE8A $_C$  and RI $\alpha_{AB}$  are rendered in surface representation in Fig. 9, A and B, respectively.

In our computational experiment, we first docked RI $\alpha$  as a rigid unit. Upon inspection of the solutions, it was clear that the two cAMP-binding domains cannot be made simultaneously accessible to the catalytic sites of PDEs (data not shown). It is conceivable that one of the RI $\alpha$  cAMP-binding domains acts first; after it extracts the cAMP, it is released, which enables the other cAMP-binding domain to bind to PDE. However, because the cAMP-binding domains in RI $\alpha$  are highly homologous, and the linker C-helix is highly dynamic (65), we proceeded to investigate whether the geometry of the two proteins, aided

with some flexibility in the central helix of RI $\alpha$ , could allow simultaneous docking of the two domains. Thus, in subsequent docking experiments, the two domains of RI $\alpha$  were docked onto the PDE8 dimer individually. The high structural similarity of the two domains suggests that they could also bind to each of the PDE8 catalytic sites in a quasi-symmetrical way.

It should be kept in mind that the scoring, and even more so the ranking, in the computational reconstruction of protein complexes remains problematic (67). Thus, we used docking to generate geometrically feasible models of the interaction proposed in this study, and used the HADDOCK's native score as guidance, but also as only one of the constraints that the model should satisfy. The chosen pose for CNB-B domain has the best HADDOCK score of  $-37.55$ , whereas CNB-A with a HADDOCK score of  $43.29$  belongs to the top 8% in its class (Fig. 9 C). The number of intervening atoms (from Criterion 2, described earlier in text) for CNB-B was among the top 3%, smallest in the 200 chosen poses, and for CNB-A among the top 30%, suggesting that the degree of the conformational change might be still larger than indicated by the model.

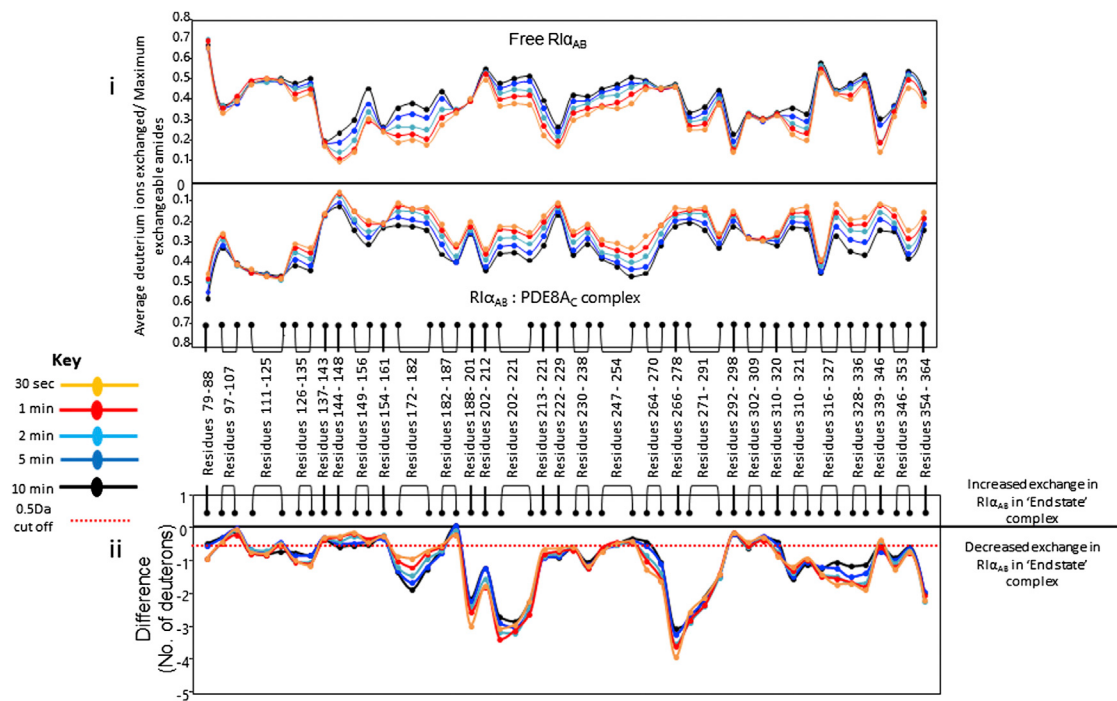


**FIGURE 6** Proteinwide overview of interaction of PDE8A $_C$  on RI $\alpha_{AB}$ . (i) Mirror plot representation for comparative analysis of HDXMS of free RI $\alpha_{AB}$  bound to PDE8A $_C$ . In this plot, relative deuterium exchange (y axis) of free RI $\alpha_{AB}$  (upper half) is compared with relative deuterium exchange of RI $\alpha_{AB}$  complexed to PDE8A $_C$  (lower half). Difference plot (ii) shows the difference in absolute number of deuterons exchanged between the two states. Negative values indicate decreased exchange upon complexation with PDE8A $_C$ . Plots were generated using the software DYNAMX (Ver. 2.0, Waters). Each point represents a pepsin digest fragment and brackets group overlapping fragment peptides.

## DISCUSSION

In this study, we report the description of a signaling complex of PDEs with PKA RI $\alpha$  through a combination of orthogonal experimental and computational approaches. This constitutes a fundamental signaling complex in the termination or resetting phase of cAMP signaling. Our results support a universal model for how PDEs bind both CNB domains of RI $\alpha$  and catalyze hydrolysis of bound cAMP leading to signal termination, with broad conservation from *Dictyostelia* to mammals.

### PDE-PKAR-subunit complex by HDXMS and computational docking suggests active site coupling mediates PDE-mediated cAMP dissociation

HDXMS studies of PDE:PKAR complexes localized the interactions to span the cAMP-binding pockets of PKA RI $\alpha$  and the regions lining the catalytic site of PDEs. This has been observed in evolutionarily distant PDEs tested, namely RegA and the full-length and catalytic domain fragment of mammalian PDE8A. Although we have chosen to focus on PDE8A for mapping interactions with PKA RI $\alpha$ , our experimental studies do not preclude similar interactions with other PDE families. The interaction interface for RI $\alpha$  on RegA is highly conserved among

all PDEs, including the cGMP-specific PDEs. Our computational model is relevant for modeling interactions with PKA RI $\alpha$  of other PDE catalytic domains as well. On PDE8A, residues that showed decreased deuterium exchange were mostly located proximal to the catalytic pocket or were residues involved in dimerization (Fig. 9 A). RI $\alpha$ , on the other hand, showed proteinwide decreases in deuterium exchange across several regions upon complexation with PDE8A $_C$  as seen in Fig. 9 B. These include the cAMP-binding pockets in both CNB-A and CNB-B, the N-terminal helical subdomain, and the interdomain helical connector regions. However, in the cAMP-bound state, large decreases in exchange are seen mainly at the cAMP-binding pockets at CNB-A and CNB-B with little effects at other regions. These two states thus represent two distinct end-point conformations of RI $\alpha$  consistent with our results from docking.

Computational docking guided by results from HDXMS provides a model for the PKA RI $\alpha$ :PDE8 interface. This solution was readily generated through docking with minimal rearrangements in the interdomain linker of RI $\alpha$ . Given the intrinsic ability of RI $\alpha$  to toggle between multiple conformational states (33), and the high dynamics of the interdomain C-helix, such a rearrangement is likely through conformational selection. This work highlights how computational docking with HDXMS and fluorescence spectroscopy can enable rapid mapping of the

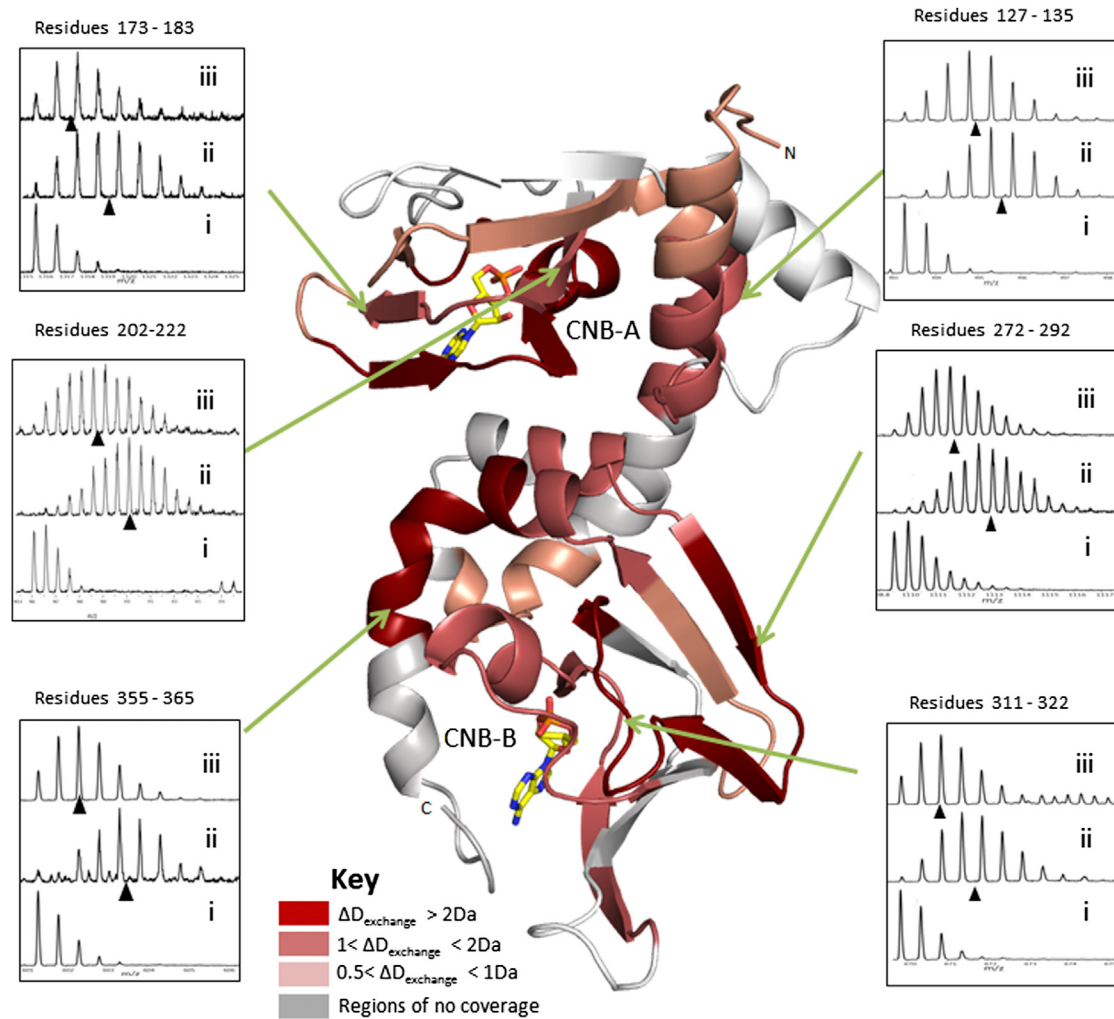


**FIGURE 7** Map of the interactions of PDE8A<sub>C</sub> on RIα<sub>AB</sub>. A summary of results from the HDXMS analysis is mapped onto the structure of cAMP-bound RIα(113–379) (PDB:1RGS). (Red shading, per key) Regions in RIα(113–379) that show significant reduction in deuterium exchange upon complex formation. (Stick representation) cAMP (C, yellow, O, red, N, blue). Mass spectra of peptides showing significant changes upon PDE8A<sub>C</sub> complex formation (difference >1 Da) are shown. The isotopic envelopes of pepsin fragment peptides of (i) undeuterated control of RIα<sub>AB</sub>, (ii) free RIα<sub>AB</sub> after 2 min deuterium exchange, and (iii) RIα<sub>AB</sub> in a complex with PDE8A<sub>C</sub> after 2 min deuterium exchange are depicted. Centroids are indicated (▲).

dynamics of transient interactions in multiprotein signaling complexes.

Analysis of HDXMS data and the docking model reveals that highly conserved residues responsible for substrate recognition are at a close proximal distance to the cAMP that is bound to RIα. This provides a model for mechanism of action, whereby active site coupling between the PDE and RIα engages residues important for cAMP binding and allostery, thereby weakening key hydrogen bonds between RIα and cAMP. The cAMP released from RIα is subsequently captured by substrate recognition residues on PDE and is channeled into the active site to be hydrolyzed into 5'AMP (Fig. 9 C, inset). The model shown here is that of monomeric RIα<sub>AB</sub> in complex with the PDE8A<sub>C</sub> dimer. This can be extended to model dimeric full-length RIα in complex with two dimers of full-length PDE. We recognize

that these results are specific to the truncation mutant of RIα and catalytic domain of PDE8A, and that the presence of additional regulatory domains might modulate PDE:PKA interactions. PDE8 has been found to interact with PKA C-subunit substrates to facilitate their phosphorylation (68), and the PDE8A:RIα complex we have described further highlights the multiple roles of PDE8 in modulating the cAMP:PKA pathway.

### How do enzymes access caged substrates?

*Phosphodiesterase binding facilitates cAMP dissociation from the PKA R-subunit and catalyzes cAMP hydrolysis*

An important question that is relevant to cAMP signaling is in understanding how cAMP tightly bound to the PKA

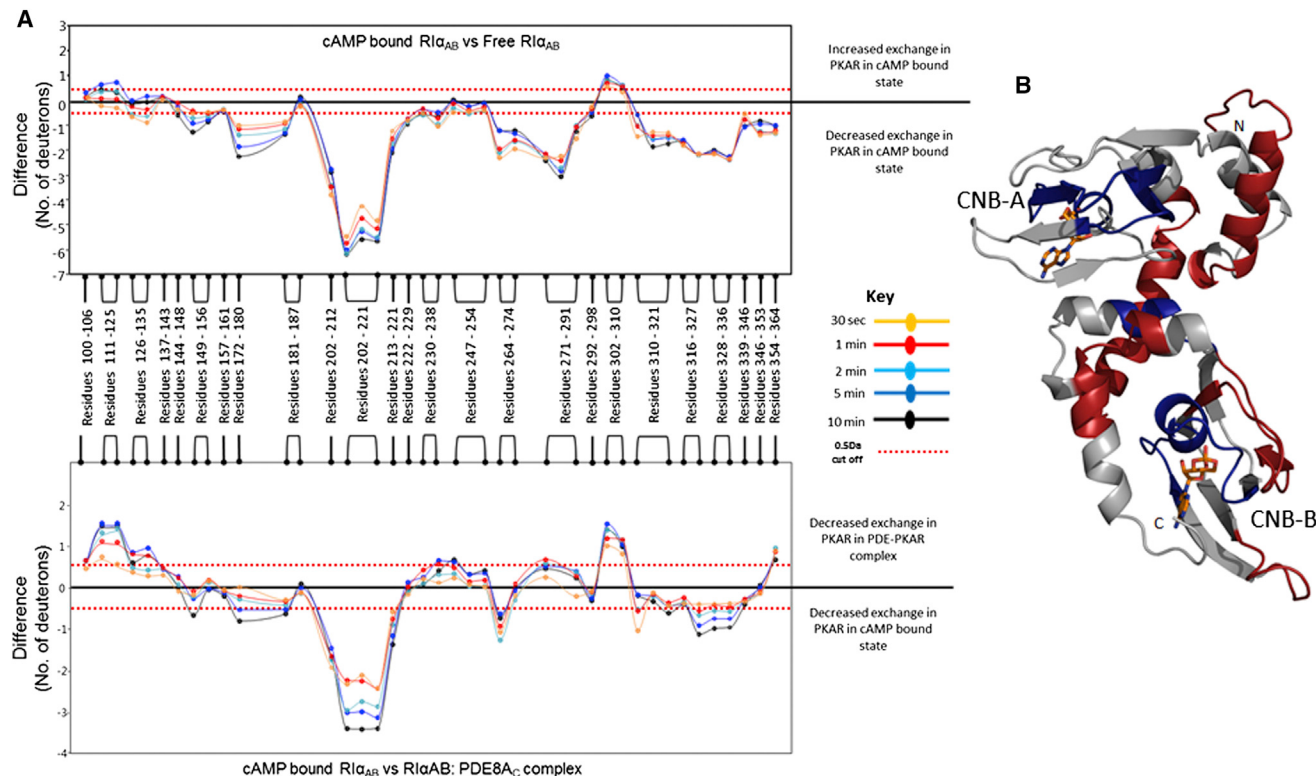


**FIGURE 8** RI $\alpha_{AB}$  adopts distinct conformations in cAMP-bound and end-state complex forms. **(A) (Top panel)** Difference plot comparing RI $\alpha_{AB}$  in the cAMP-bound state to the apo state. Peptides in the positive range represent increased deuterium exchange in the cAMP-bound state as compared to the apo state, whereas peptides in the negative range represent cAMP-induced protection. **(Bottom panel)** Difference plot comparing RI $\alpha_{AB}$  in the cAMP-bound state to the end-state complex. Peptides in the positive range indicate peptides showing decreased deuterium exchange in the end-state complex in comparison to the apo state, whereas peptides in the negative range represent peptides showing decreased deuterium exchange in the cAMP-bound state in comparison to the end-state complex. Peptide residue numbers, from the N- to C-terminal of RI $\alpha_{AB}$ , are marked along the x axis; absolute difference in Da is marked along the y axis. Each point represents a pepsin digest fragment and brackets group overlapping fragment peptides. Deuterium exchange labeling times are colored according to key. **(B)** Results from the cAMP-bound state versus the end-state complex difference plot were plotted onto the structure of RI $\alpha$  (PDB:1RGS). **(Red regions)** Greater protection in the end-state complex; **(blue regions)** greater protection in the cAMP-bound state. **(Orange sticks)** cAMP molecules, bound to CNB-A and CNB-B.

R-subunit is accessed by PDEs and hydrolyzed to reset the PKA signaling system. cAMP is anchored within the target R-subunit by a network of salt bridges and H-bonds, thereby binding it with high affinity. By binding to cAMP with very high affinity, PKA R-subunits function as buffers for cAMP. The cAMP can thus be considered analogous to a caged substrate that must first undergo dissociation before it can be accessed by PDEs for hydrolysis. It is therefore possible that PDE function must encompass hydrolyzing both caged and unbound cytosolic cAMP.

Our results demonstrate how PDE8A binds RI $\alpha$  and provides a model for how it facilitates dissociation of cAMP from both target CNB domains, highlighting how PKA RI $\alpha$  might serve to buffer intracellular cAMP and channel it to the active site of PDE8A. Substrate channeling is characteristic of metabolic enzymes (69), but is being proposed here for the first time in cAMP signaling. Sequestering of cAMP-bound RI $\alpha$  by PDEs has important implications. This allows for localized pools of cAMP to activate PKA in microdomains. It also facilitates adaptation to steady-state levels of cAMP by completing the cAMP cycle

through regeneration of the inactive holoenzyme. This also ensures that reactivation of PKA would occur preferentially upon large fluxes of cAMP levels in the cell (70). PDE:PKA RI $\alpha$  interactions described are only likely to be enhanced further by AKAPs.

## SUPPORTING MATERIAL

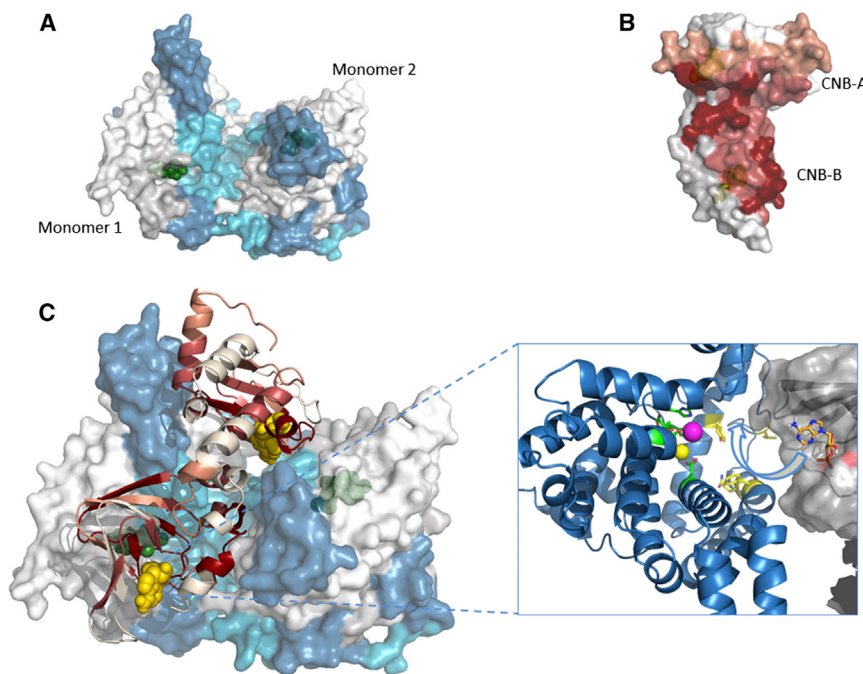
Six figures, two tables and additional supporting information are available at [http://www.biophysj.org/biophysj/supplemental/S0006-3495\(14\)00796-6](http://www.biophysj.org/biophysj/supplemental/S0006-3495(14)00796-6).

The authors thank Dr. Susan Taylor, University of California at San Diego, and Cecilia Cheng in the Taylor laboratory, for enabling use of and technical assistance with peptide arrays. We also thank Dr. Joseph Beavo, University of Washington for feedback and helpful discussions.

This work was supported by grants from Ministry of Education (No. MOE2012-T3-1-008), Singapore to G.S.A. and I.M., Mechanobiology Institute, National University of Singapore, Singapore, and a grant from Waters Corporation to G.S.A.

## SUPPORTING CITATIONS

References (71-77) appear in the Supporting Material.



(only cAMP:A domain, residues 113–244, shown for clarity). A single chain of PDE8A (chain A) alone has been hidden to enable a clear view of the active site. PDE binding mediates dissociation of the phosphate of cAMP from RI $\alpha$  (indicated by arrow).

## REFERENCES

- Rehmann, H., A. Rueppel, ..., A. Wittinghofer. 2003. Communication between the regulatory and the catalytic region of the cAMP-responsive guanine nucleotide exchange factor Epac. *J. Biol. Chem.* 278:23508–23514.
- Kamenetsky, M., S. Middelhaufe, ..., C. Steegborn. 2006. Molecular details of cAMP generation in mammalian cells: a tale of two systems. *J. Mol. Biol.* 362:623–639.
- Conti, M., and J. Beavo. 2007. Biochemistry and physiology of cyclic nucleotide phosphodiesterases: essential components in cyclic nucleotide signaling. *Annu. Rev. Biochem.* 76:481–511.
- Rich, T. C., K. A. Fagan, ..., J. W. Karpen. 2001. A uniform extracellular stimulus triggers distinct cAMP signals in different compartments of a simple cell. *Proc. Natl. Acad. Sci. USA*. 98:13049–13054.
- Steinberg, S. F., and L. L. Brunton. 2001. Compartmentation of G protein-coupled signaling pathways in cardiac myocytes. *Annu. Rev. Pharmacol. Toxicol.* 41:751–773.
- Baillie, G. S., D. R. Adams, ..., M. D. Houslay. 2007. Mapping binding sites for the PDE4D5 cAMP-specific phosphodiesterase to the N- and C-domains of  $\beta$ -arrestin using spot-immobilized peptide arrays. *Biochem. J.* 404:71–80.
- Baillie, G. S., E. Huston, ..., M. D. Houslay. 2002. TAPAS-1, a novel microdomain within the unique N-terminal region of the PDE4A1 cAMP-specific phosphodiesterase that allows rapid,  $\text{Ca}^{2+}$ -triggered membrane association with selectivity for interaction with phosphatidic acid. *J. Biol. Chem.* 277:28298–28309.
- Bolger, G. B., G. S. Baillie, ..., M. D. Houslay. 2006. Scanning peptide array analyses identify overlapping binding sites for the signaling scaffold proteins,  $\beta$ -arrestin and RACK1, in cAMP-specific phosphodiesterase PDE4D5. *Biochem. J.* 398:23–36.
- Huston, E., I. Gall, ..., M. D. Houslay. 2006. Helix-1 of the cAMP-specific phosphodiesterase PDE4A1 regulates its phospholipase-D-dependent redistribution in response to release of  $\text{Ca}^{2+}$ . *J. Cell Sci.* 119:3799–3810.
- Smith, K. J., G. S. Baillie, ..., M. D. Houslay. 2007.  $^1\text{H}$  NMR structural and functional characterization of a cAMP-specific phosphodiesterase-4D5 (PDE4D5) N-terminal region peptide that disrupts PDE4D5 interaction with the signaling scaffold proteins,  $\beta$ -arrestin and RACK1. *Cell. Signal.* 19:2612–2624.
- Houslay, M. D. 2010. Underpinning compartmentalized cAMP signaling through targeted cAMP breakdown. *Trends Biochem. Sci.* 35:91–100.
- Houslay, M. D., G. S. Baillie, and D. H. Maurice. 2007. cAMP-specific phosphodiesterase-4 enzymes in the cardiovascular system: a molecular toolbox for generating compartmentalized cAMP signaling. *Circ. Res.* 100:950–966.
- Keravis, T., and C. Lugnier. 2010. Cyclic nucleotide phosphodiesterases (PDE) and peptide motifs. *Curr. Pharm. Des.* 16:1114–1125.
- Davare, M. A., V. Avdonin, ..., J. W. Hell. 2001. A  $\beta 2$  adrenergic receptor signaling complex assembled with the  $\text{Ca}^{2+}$  channel Cav1.2. *Science*. 293:98–101.
- Berman, H. M., L. F. Ten Eyck, ..., S. S. Taylor. 2005. The cAMP binding domain: an ancient signaling module. *Proc. Natl. Acad. Sci. USA*. 102:45–50.
- Taylor, S. S., C. Kim, ..., G. S. Anand. 2005. Dynamics of signaling by PKA. *Biochim. Biophys. Acta*. 1754:25–37.
- Das, R., V. Esposito, ..., G. Melacini. 2007. cAMP activation of PKA defines an ancient signaling mechanism. *Proc. Natl. Acad. Sci. USA*. 104:93–98.
- Johnson, D. A., P. Akamine, ..., S. S. Taylor. 2001. Dynamics of cAMP-dependent protein kinase. *Chem. Rev.* 101:2243–2270.
- Kim, C., C. Y. Cheng, ..., S. S. Taylor. 2007. PKA-I holoenzyme structure reveals a mechanism for cAMP-dependent activation. *Cell*. 130:1032–1043.
- Kim, C., N. H. Xuong, and S. S. Taylor. 2005. Crystal structure of a complex between the catalytic and regulatory (RI $\alpha$ ) subunits of PKA. *Science*. 307:690–696.

21. Su, Y., W. R. Dostmann, ..., K. I. Varughese. 1995. Regulatory subunit of protein kinase A: structure of deletion mutant with cAMP binding domains. *Science*. 269:807–813.
22. Abu-Abed, M., R. Das, ..., G. Melacini. 2007. Definition of an electrostatic relay switch critical for the cAMP-dependent activation of protein kinase A as revealed by the D170A mutant of RIα. *Proteins*. 69:112–124.
23. Byeon, I. J., K. K. Dao, ..., A. M. Gronenborn. 2010. Allosteric communication between cAMP binding sites in the RI subunit of protein kinase A revealed by NMR. *J. Biol. Chem.* 285:14062–14070.
24. Das, R., M. Abu-Abed, and G. Melacini. 2006. Mapping allosteric through equilibrium perturbation NMR spectroscopy. *J. Am. Chem. Soc.* 128:8406–8407.
25. Das, R., S. Chowdhury, ..., G. Melacini. 2009. Dynamically driven ligand selectivity in cyclic nucleotide binding domains. *J. Biol. Chem.* 284:23682–23696.
26. Das, R., M. T. Mazhab-Jafari, ..., G. Melacini. 2008. Entropy-driven cAMP-dependent allosteric control of inhibitory interactions in exchange proteins directly activated by cAMP. *J. Biol. Chem.* 283:19691–19703.
27. Das, R., and G. Melacini. 2007. A model for agonism and antagonism in an ancient and ubiquitous cAMP-binding domain. *J. Biol. Chem.* 282:581–593.
28. McNicholl, E. T., R. Das, ..., G. Melacini. 2010. Communication between tandem cAMP binding domains in the regulatory subunit of protein kinase A- $\text{I}\alpha$  as revealed by domain-silencing mutations. *J. Biol. Chem.* 285:15523–15537.
29. Anand, G. S., M. Hotchko, ..., S. S. Taylor. 2007. R-subunit isoform specificity in protein kinase A: distinct features of protein interfaces in PKA types I and II by amide H/2H exchange mass spectrometry. *J. Mol. Biol.* 374:487–499.
30. Anand, G. S., C. A. Hughes, ..., E. A. Komives. 2002. Amide H/2H exchange reveals communication between the cAMP and catalytic subunit-binding sites in the RIα subunit of protein kinase A. *J. Mol. Biol.* 323:377–386.
31. Hamuro, Y., G. S. Anand, ..., V. L. Woods, Jr. 2004. Mapping intersubunit interactions of the regulatory subunit (RIα) in the type I holoenzyme of protein kinase A by amide hydrogen/deuterium exchange mass spectrometry (DXMS). *J. Mol. Biol.* 340:1185–1196.
32. Anand, G. S., S. Krishnamurthy, ..., D. A. Johnson. 2010. Cyclic AMP- and (Rp)-cAMP-induced conformational changes in a complex of the catalytic and regulatory (RIα) subunits of cyclic AMP-dependent protein kinase. *Mol. Cell. Proteomics*. 9:2225–2237.
33. Badireddy, S., G. Yunfeng, ..., G. S. Anand. 2011. Cyclic AMP analog blocks kinase activation by stabilizing inactive conformation: conformational selection highlights a new concept in allosteric inhibitor design. *Mol. Cell. Proteomics*. 10: M110-004390.
34. Boehr, D. D., R. Nussinov, and P. E. Wright. 2009. The role of dynamic conformational ensembles in biomolecular recognition. *Nat. Chem. Biol.* 5:789–796.
35. Changeux, J. P. 2012. Allostery and the Monod-Wyman-Changeux model after 50 years. *Annu. Rev. Biophys.* 41:103–133.
36. Moorthy, B. S., S. Badireddy, and G. S. Anand. 2011. Cooperativity and allostery in cAMP-dependent activation of protein kinase A: monitoring conformations of intermediates by amide hydrogen/deuterium exchange. *Int. J. Mass Spectrom.* 302:157–166.
37. Herberg, F. W., W. R. Dostmann, ..., S. S. Taylor. 1994. Crosstalk between domains in the regulatory subunit of cAMP-dependent protein kinase: influence of amino terminus on cAMP binding and holoenzyme formation. *Biochemistry*. 33:7485–7494.
38. Moorthy, B. S., Y. Gao, and G. S. Anand. 2011. Phosphodiesterases catalyze hydrolysis of cAMP-bound to regulatory subunit of protein kinase A and mediate signal termination. *Mol. Cell. Proteomics*. 10: M110-002295.
39. Shaulsky, G., D. Fuller, and W. F. Loomis. 1998. A cAMP-phosphodiesterase controls PKA-dependent differentiation. *Development*. 125:691–699.
40. Krishnamurthy, S., B. S. Moorthy, ..., G. S. Anand. 2013. Dynamics of phosphodiesterase-induced cAMP dissociation from protein kinase A: capturing transient ternary complexes by HDXMS. *Biochim. Biophys. Acta*. 1834:1215–1221.
41. Corbin, J. D., P. H. Sugden, ..., D. McCarthy. 1978. Studies on the properties and mode of action of the purified regulatory subunit of bovine heart adenosine 3':5'-monophosphate-dependent protein kinase. *J. Biol. Chem.* 253:3997–4003.
42. Døskeland, S. O. 1978. Evidence that rabbit muscle protein kinase has two kinetically distinct binding sites for adenosine 3':5'-cyclic monophosphate. *Biochem. Biophys. Res. Commun.* 83:542–549.
43. Dodge, K. L., S. Khouangtsathiene, ..., J. D. Scott. 2001. mAKAP assembles a protein kinase A/PDE4 phosphodiesterase cAMP signaling module. *EMBO J.* 20:1921–1930.
44. Edwards, H. V., J. D. Scott, and G. S. Baillie. 2012. The A-kinase-anchoring protein AKAP-Lbc facilitates cardioprotective PKA phosphorylation of Hsp20 on Ser<sup>16</sup>. *Biochem. J.* 446:437–443.
45. Lynch, M. J., G. S. Baillie, ..., M. D. Houslay. 2005. RNA silencing identifies PDE4D5 as the functionally relevant cAMP phosphodiesterase interacting with β arrestin to control the protein kinase A/ AKAP79-mediated switching of the β2-adrenergic receptor to activation of ERK in HEK293B2 cells. *J. Biol. Chem.* 280:33178–33189.
46. McCahill, A., T. McSorley, ..., M. D. Houslay. 2005. In resting COS1 cells a dominant negative approach shows that specific, anchored PDE4 cAMP phosphodiesterase isoforms gate the activation, by basal cyclic AMP production, of AKAP-tethered protein kinase A type II located in the centrosomal region. *Cell. Signal.* 17:1158–1173.
47. Anand, G. S., D. Law, ..., E. A. Komives. 2003. Identification of the protein kinase A regulatory RIα-catalytic subunit interface by amide H/2H exchange and protein docking. *Proc. Natl. Acad. Sci. USA*. 100:13264–13269.
48. Pandit, D., S. J. Tuske, ..., Y. Hamuro. 2012. Mapping of discontinuous conformational epitopes by amide hydrogen/deuterium exchange mass spectrometry and computational docking. *J. Mol. Rec.* 25:114–124.
49. Roberts, V. A., M. E. Pique, ..., V. L. Woods, Jr. 2012. Combining H/D exchange mass spectrometry and computational docking reveals extended DNA-binding surface on uracil-DNA glycosylase. *Nucleic Acids Res.* 40:6070–6081.
50. Yan, Z., H. Wang, ..., H. Ke. 2009. Refolding and kinetic characterization of the phosphodiesterase-8A catalytic domain. *Protein Expr. Purif.* 64:82–88.
51. Diller, T. C., N. H. Xuong, and S. S. Taylor. 2000. Type II β-regulatory subunit of cAMP-dependent protein kinase: purification strategies to optimize crystallization. *Protein Expr. Purif.* 20:357–364.
52. Anand, G., S. S. Taylor, and D. A. Johnson. 2007. Cyclic-AMP and pseudosubstrate effects on type-I A-kinase regulatory and catalytic subunit binding kinetics. *Biochemistry*. 46:9283–9291.
53. Buechler, Y. J., and S. S. Taylor. 1991. Mutations in the autoinhibitor site of the regulatory subunit of cAMP-dependent protein kinase I. Replacement of Ala-97 and Ser-99 interferes with reassociation with the catalytic subunit. *J. Biol. Chem.* 266:3491–3497.
54. Wales, T. E., K. E. Fadgen, ..., J. R. Engen. 2008. High-speed and high-resolution UPLC separation at zero degrees Celsius. *Anal. Chem.* 80:6815–6820.
55. Bateman, R. H., R. Carruthers, ..., J. P. Vissers. 2002. A novel precursor ion discovery method on a hybrid quadrupole orthogonal acceleration time-of-flight (Q-TOF) mass spectrometer for studying protein phosphorylation. *J. Am. Soc. Mass Spectrom.* 13:792–803.
56. Silva, J. C., R. Denny, ..., S. Geromanos. 2005. Quantitative proteomic analysis by accurate mass retention time pairs. *Anal. Chem.* 77:2187–2200.
57. Geromanos, S. J., J. P. Vissers, ..., J. I. Langridge. 2009. The detection, correlation, and comparison of peptide precursor and product ions from data independent LC-MS with data dependant LC-MS/MS. *Proteomics*. 9:1683–1695.

58. Shen, Z., P. Li, ..., B. C. Wang. 2009. Label-free quantitative proteomics analysis of etiolated maize seedling leaves during greening. *Mol. Cell. Proteomics.* 8:2443–2460.
59. Dominguez, C., R. Boelens, and A. M. Bonvin. 2003. HADDOCK: a protein-protein docking approach based on biochemical or biophysical information. *J. Am. Chem. Soc.* 125:1731–1737.
60. Arnold, K., L. Bordoli, ..., T. Schwede. 2006. The SWISS-MODEL workspace: a web-based environment for protein structure homology modeling. *Bioinformatics.* 22:195–201.
61. Wang, H., Z. Yan, ..., H. Ke. 2008. Kinetic and structural studies of phosphodiesterase-8A and implication on the inhibitor selectivity. *Biochemistry.* 47:12760–12768.
62. Thomason, P. A., D. Traynor, ..., R. R. Kay. 1998. An intersection of the cAMP/PKA and two-component signal transduction systems in *Dictyostelium*. *EMBO J.* 17:2838–2845.
63. Poppe, H., S. D. Rybalkin, ..., E. Butt. 2008. Cyclic nucleotide analogs as probes of signaling pathways. *Nat. Methods.* 5:277–278.
64. Akimoto, M., R. Selvaratnam, ..., G. Melacini. 2013. Signaling through dynamic linkers as revealed by PKA. *Proc. Natl. Acad. Sci. USA.* 110:14231–14236.
65. Kornev, A. P., S. S. Taylor, and L. F. Ten Eyck. 2008. A generalized allosteric mechanism for *cis*-regulated cyclic nucleotide binding domains. *PLOS Comput. Biol.* 4:e1000056.
66. Selvaratnam, R., S. Chowdhury, ..., G. Melacini. 2011. Mapping allostericity through the covariance analysis of NMR chemical shifts. *Proc. Natl. Acad. Sci. USA.* 108:6133–6138.
67. Lensink, M. F., and S. J. Wodak. 2010. Docking and scoring protein interactions: CAPRI 2009. *Proteins.* 78:3073–3084.
68. Brown, K. M., J. P. Day, ..., G. S. Baillie. 2013. Phosphodiesterase-8A binds to and regulates Raf-1 kinase. *Proc. Natl. Acad. Sci. USA.* 110:E1533–E1542.
69. Huang, X., H. M. Holden, and F. M. Raushel. 2001. Channeling of substrates and intermediates in enzyme-catalyzed reactions. *Annu. Rev. Biochem.* 70:149–180.
70. Leiser, M., N. Fleischer, and J. Erlichman. 1986. Enhanced activation of cAMP-dependent protein kinase by rapid synthesis and degradation of cAMP. *J. Biol. Chem.* 261:15486–15490.
71. Burns-Hamuro, L. L., Y. Ma, ..., S. S. Taylor. 2003. Designing isoform-specific peptide disruptors of protein kinase A localization. *Proc. Natl. Acad. Sci. USA.* 100:4072–4077.
72. Sathyaranayana, P., E. Houde, ..., D. M. Wojchowski. 2009. CNTO 530 functions as a potent EPO mimetic via unique sustained effects on bone marrow proerythroblast pools. *Blood.* 113:4955–4962.
73. Bogacheva, O., O. Bogachev, ..., D. M. Wojchowski. 2008. DYRK3 dual-specificity kinase attenuates erythropoiesis during anemia. *J. Biol. Chem.* 283:36665–36675.
74. Mandell, J. G., A. Baerga-Ortiz, ..., E. A. Komives. 2001. Solvent accessibility of the thrombin-thrombomodulin interface. *J. Mol. Biol.* 306:575–589.
75. Houde, D., S. A. Berkowitz, and J. R. Engen. 2011. The utility of hydrogen/deuterium exchange mass spectrometry in biopharmaceutical comparability studies. *J. Pharm. Sci.* 100:2071–2086.
76. Wojchowski, D. M., M. P. Menon, ..., O. Bogachev. 2006. Erythropoietin-dependent erythropoiesis: new insights and questions. *Blood Cells Mol. Dis.* 36:232–238.
77. Pikitch, E. K., C. Santora, ..., K. J. Sainsbury. 2004. Ecology. Ecosystem-based fishery management. *Science.* 305:346–347.

Active Site Coupling in PDE-PKA Complexes promotes Resetting of Mammalian  
cAMP Signaling \*

**Srinath Krishnamurthy<sup>1,2</sup>, Balakrishnan Shenbaga Moorthy<sup>1</sup>, Lim Xin Xiang<sup>1</sup>, Lim Xin Shan<sup>1</sup>, Kavitha Bharatham<sup>3</sup>, Nikhil Kumar Tulsian<sup>1</sup>, Ivana Mihalek<sup>3</sup> and Ganesh S. Anand\*<sup>1,2</sup>**

<sup>1</sup>Department of Biological Sciences National University of Singapore, 14 Science Dr 4,  
Singapore 117543

<sup>2</sup>Mechanobiology Institute, National University of Singapore

<sup>3</sup>Bioinformatics Institute, A\*Star, 30 Biopolis Street, #07-01 Matrix,  
Singapore 13867

## Supplementary Information

**Peptide Array Analysis identifies locus of contiguous RegA:RIα Interactions:** We applied peptide array analysis to independently probe the binding site for full-length RIα on RegA. A library of overlapping peptides of 15-mers from the primary sequence of RegA, each frameshifted by 5 amino acids was synthesized and immobilized on a cellulose membrane (A2 to D8 in Supplementary Figure S1) as described (1). The cellulose membrane was then incubated with cAMP-free full length RIα followed by extensive washing. The bound RIα was then detected with RIα specific antibodies followed by secondary antibodies similar to immunoblotting assays (2). Dark spots reflect direct interaction sites with RIα, summarized in the table (Supplementary Figure S1). To minimize false positive results, we only considered overlapping peptides where binding to RIα was detected (3). Analysis of the modeled structure of RegA based on that of PDE8A showed that the two overlapping sets of interacting peptides are contiguous. Consecutive peptides showing positive interactions span residues 516-540 important for divalent metal binding and catalysis. A second region included overlapping peptides 556-570, 561-575 and 566-580 that together with the first set highlights the linear loci for interactions with the CNB:A domain of RIα (Figure 2B).

**HDXMS analysis of RIα CNB:A-RegAc interaction:** To map the interface on RegA that interacted with the CNB:A domain of RIα (4), we carried out HDXMS on the RIα<sub>A</sub>:RegAc complex. Prior to deuterium exchange, undeuterated samples of RegAc were subjected to complete proteolysis by pepsin, followed by peptide sequencing and identification as described in materials and methods (4). Overall 32 peptides were detected, which covered ~ 81% of the

RegAc sequence. These were each well resolved with high signal to noise ratios ( $S/N = 6$ ) and were subsequently analyzed in the deuterium exchange experiments.

Based on the estimated  $K_D$  ( $\leq 1.6 \mu\text{M}$ ) for the RegAc-cAMP free RI $\alpha_A$  complex (4), excess cAMP-free RI $\alpha_A$  ( $60 \mu\text{M}$ ) was incubated with RegAc ( $20 \mu\text{M}$ ) to bind RegAc to saturation. Deuterium exchange was then carried out as described in materials and methods. Since the observed rate of exchange,  $k_{\text{obs}}$  is dependent on an interplay of both the dissociation constant and the intrinsic deuterium exchange rate, we factored in the upper limit of the dissociation constant to optimize the relative and absolute concentrations of both RegAc and RI $\alpha_A$ . With a 3X excess of RI $\alpha_A$  ( $60 \mu\text{M}$ ) for RegAc ( $20 \mu\text{M}$ ), we estimated complete saturation of RegAc in complex with RI $\alpha_A$  (5), enabling us to monitor the changes in RegAc upon interactions with RI $\alpha_A$ . A Difference plot (6) was used to provide a protein-wide overview of the difference in relative deuterium exchange for free and RI $\alpha_A$  bound RegAc (Supplementary Figure S2A) for a time course ranging from 0 -10 min. ESI-QTOF spectra for three peptides from RegAc which show the largest shifts in deuterium exchange (Don=10 min) upon interactions with RI $\alpha_A$  are shown in Supplementary Figure S2B. Kinetic plots of deuterium exchange for these peptides (Supplementary Figure S2C) reveal significant differences in deuterium exchange that are observable for all of the time points monitored. HDXMS results for the catalytic domain of RegA were mapped onto the homology modeled PDE structure of the closest cAMP PDE homolog of RegA, PDE8 (PDB ID: 3ECM) using SWISS-MODELLER (Figure 2A) (7, 8).

Within RegAc, the catalytically important M loop showed decreased exchange upon interactions with RI $\alpha_A$ . From multiple sequence analyses, the residues are highly conserved across the PDE superfamily and are critical for the coordination of the two divalent metal ions Zn $^{2+}$  and Mg $^{2+}$  necessary for catalysis. Interestingly HDXMS results showed that pepsin fragment peptides 525-538 and 634-642, which span catalytically important residues H527, D528 and D639 showed significantly reduced exchange upon binding RI $\alpha_A$ . Peptides spanning residues also critical for substrate cAMP recognition 525-538, 634-642, 656-661 and 668-693 showed decreased exchange upon interactions with RI $\alpha_A$ .

**Bioinformatics analysis to identify vertebrate/mammalian homolog of RegA:** Based on the interactions observed between RegAc and RI $\alpha_A$ , we set out to identify possible vertebrate/mammalian PDE homolog(s) in an equivalent mechanism for signal termination. We first set out to establish if the RegA-RI $\alpha$  interaction is specific for any particular PDE among several (~50 subtypes) human PDE subtypes. In order to investigate this, we used the following approaches:

1. Sequence comparison
  1. Comparison of protein sequences human PDE-ome (all vertebrate orthologs according to ENSEMBL database-<http://www.ensembl.org/index.html>)
    - a) with RegA
    - b) Overall conservation of vertebrate PDEs in RegA:PKA-RI $\alpha$  interaction interface based on HDXMS.
  2. Intron-exon structure comparison
    - 1. Sequence homology across the PDE superfamily**
      - a. Comparison of human PDE-ome with RegA*

Human orthologs from ENSEMBL (<http://www.ensembl.org/index.html>) database were retrieved for RegA. By looking at the overall similarity, PDE9 (which is cGMP specific) most closely resembled RegA followed by PDE8, while PDE4 turns out to be the one with maximum stretches of homology, including the regulatory domain region (Supplementary Figure S3).

*b. Overall conservation pattern in RegA:PKA-RI $\alpha$  interaction region*

We investigated whether residues identified on RegA that interacted with RI $\alpha$  on the basis of HDXMS, corresponded to regions of residue type conservation across PDE orthologs. To compare vertebrate PDEs with RegA, their sequences were aligned (by *Muscle* sequence alignment program (9)) and the conservation of residues at each position in the alignment were determined using real-valued evolutionary trace, (Fig. 2E, Supplementary Figure S4). The degree of conservation of each residue corresponds to its functional importance for the protein. Each residue is color coded based on its conservation (Supplementary Figure S4A). These include three helices in pink (Supplementary Figure S4B). Conservation pattern shows that most of these residues are well conserved across PDEs as indicated in bright yellow and red thereby suggesting that they cannot be specific for any PDE.

We then divided PDEs broadly into four subgroups: cAMP specific; cGMP specific, cAMP or cGMP binding; and RegA. Residues that are conserved within a subgroup regardless of conservation in other groups are called determinants of that subgroup while positions that are conserved within each group but not across them are termed discriminants. Detecting such positions in the RI $\alpha$  interaction interface would indicate that the binding is perhaps specific to a subfamily of PDE (Supplementary Figure S4C). As hinted from conservation analysis, we could not find any significant discriminants in the region of interest. Based on these results, it appeared very likely that all vertebrate PDEs may interact with RI $\alpha$  rather than a specific PDE alone.

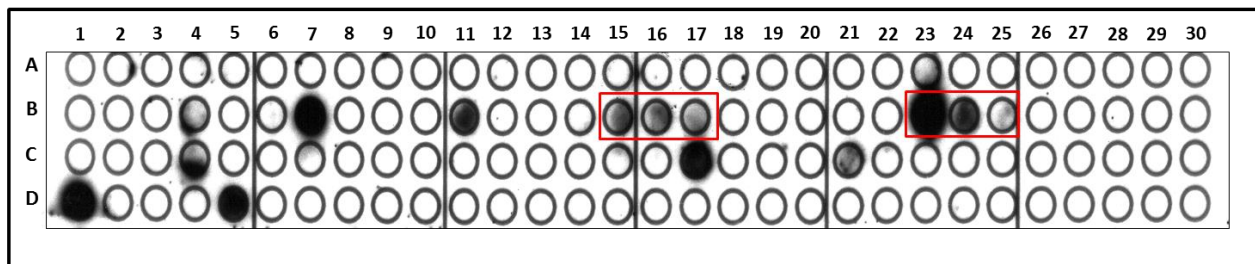
**2. Exon-intron structure of PDEs:** The evolution of intron-exon structure is independent of the evolution of the protein sequence (for example (10)). This means that it may provide independent information about evolutionary relationships among genes (and proteins they code for). We investigated the possibility of using the conservation of intron positions as an indication of closer relationship of RegA to some (cAMP/cGMP specific) vertebrate PDEs.

Among human PDEs, the intron positions within/around PKA-RI $\alpha$  binding region coincide for PDE5A and PDE6A. Other than that, we could not observe any pattern that could strongly suggest that certain PDEs resemble/differ from RegA from intron-exon structure analysis.

**Conclusion:** Bioinformatics analysis based on sequence conservation suggested that the residues binding PKA-RI $\alpha$  are well conserved across all PDEs possibly corroborated with the lack of any discriminants in the region of interest, indicating that there might possibly be more than a single PDE capable of interacting with PKA-RI $\alpha$  and the conservation at the PKA-RI $\alpha$  binding across vertebrate PDEs strongly suggests that this could well be a conserved property of all PDE types.

**Supplementary Figure:**

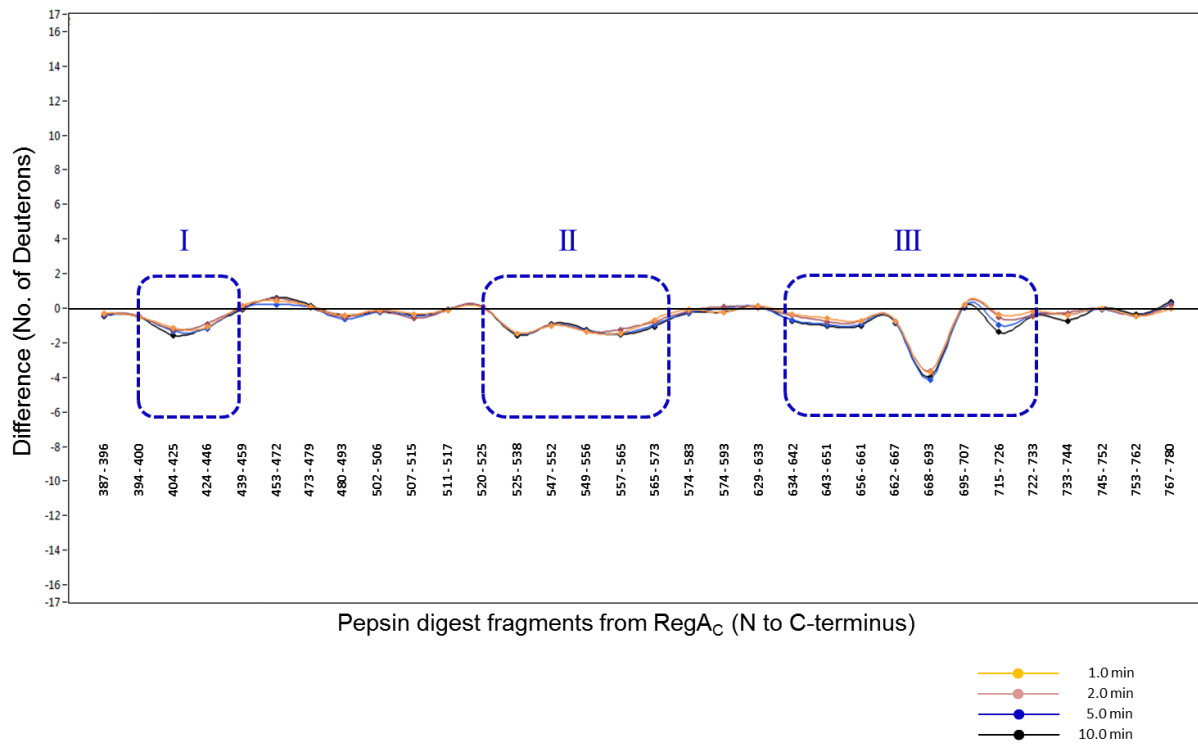
Supplementary Figure S1



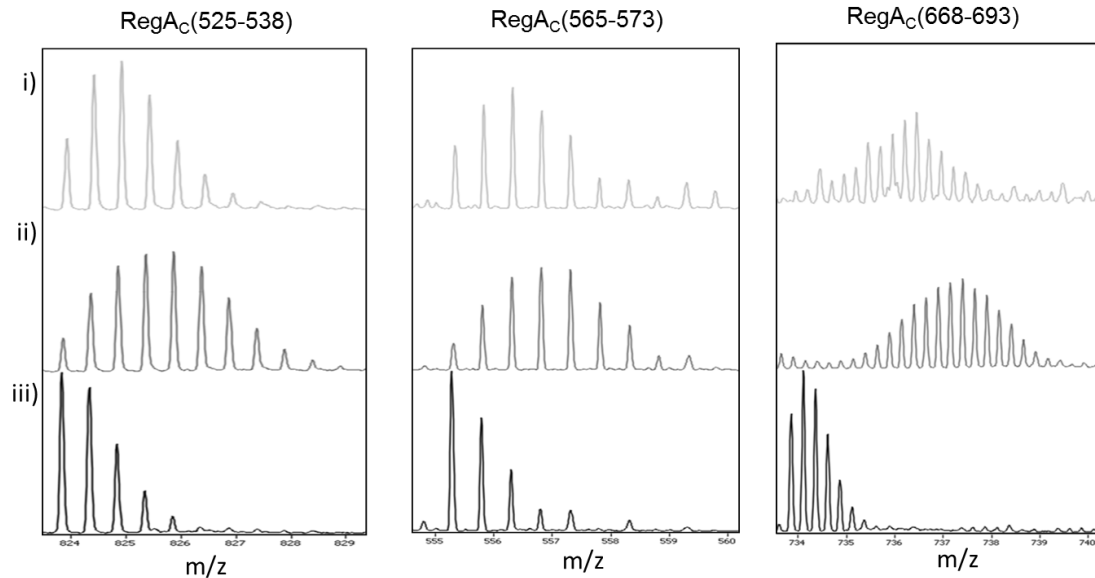
Spot No.	Peptide probe (RegA)	Residue Nos.
B15	DIFALLISCMCHDLN	516-530
B16	LISCMCHDLNHPGFN	521-535
B17	CHDLNHPGFNNNTFQV	526-540
B23	LENHHAMLTTFKILRN	556-570
B24	AMLTFKILRNSECNI	561-575
B25	KILRNSECNILEGLN	566-580

**Supplementary Figure S1: Peptide array data shows interaction of RI $\alpha$  with RegA:** Peptides that interacted with RI $\alpha$  generated dark spots in contrast to non-interacting peptide (blank spots) and peptides interacts specifically with RI $\alpha$  are shown in red box. Spot numbers (A2 to D8) relate to peptides in the scanned array (A2 to D8, spot A2 → 301-315 residues, spot A3 → 306-320 residues and so on to D8→ 781-793) and whose sequence which interacts specifically are listed in the table.

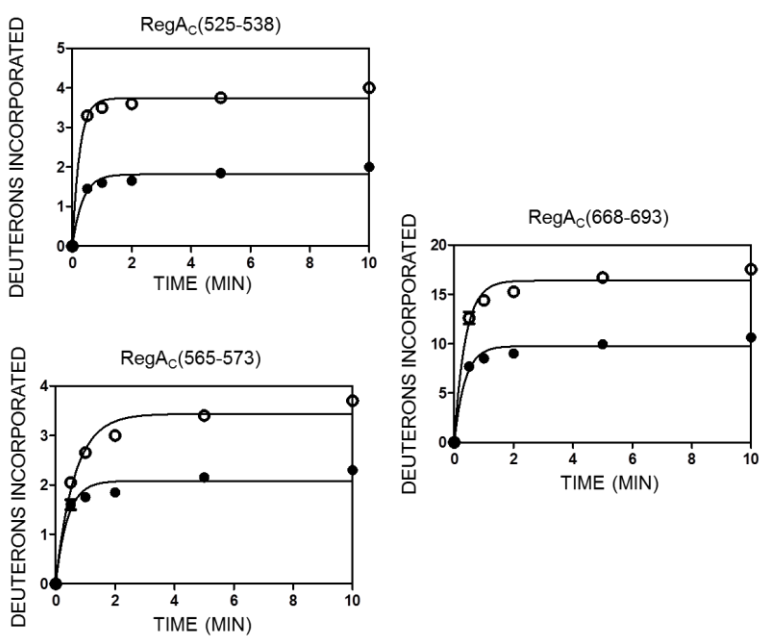
Supplementary Figure S2A



Supplementary Figure S2B

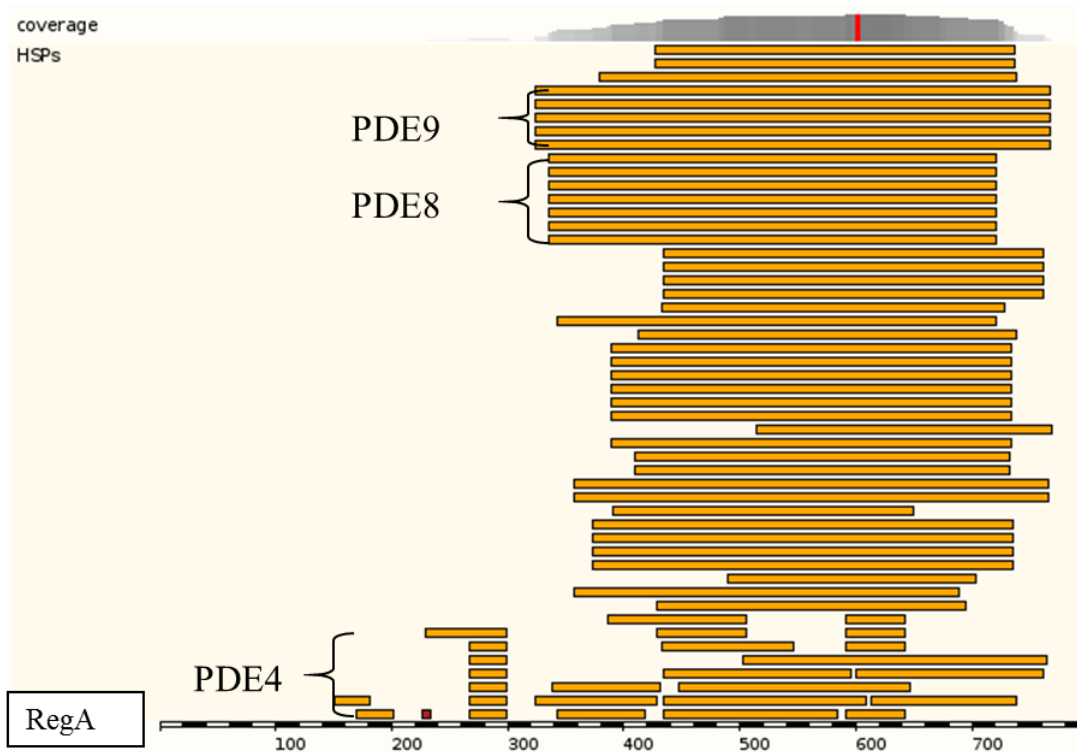


Supplementary  
Figure S2C



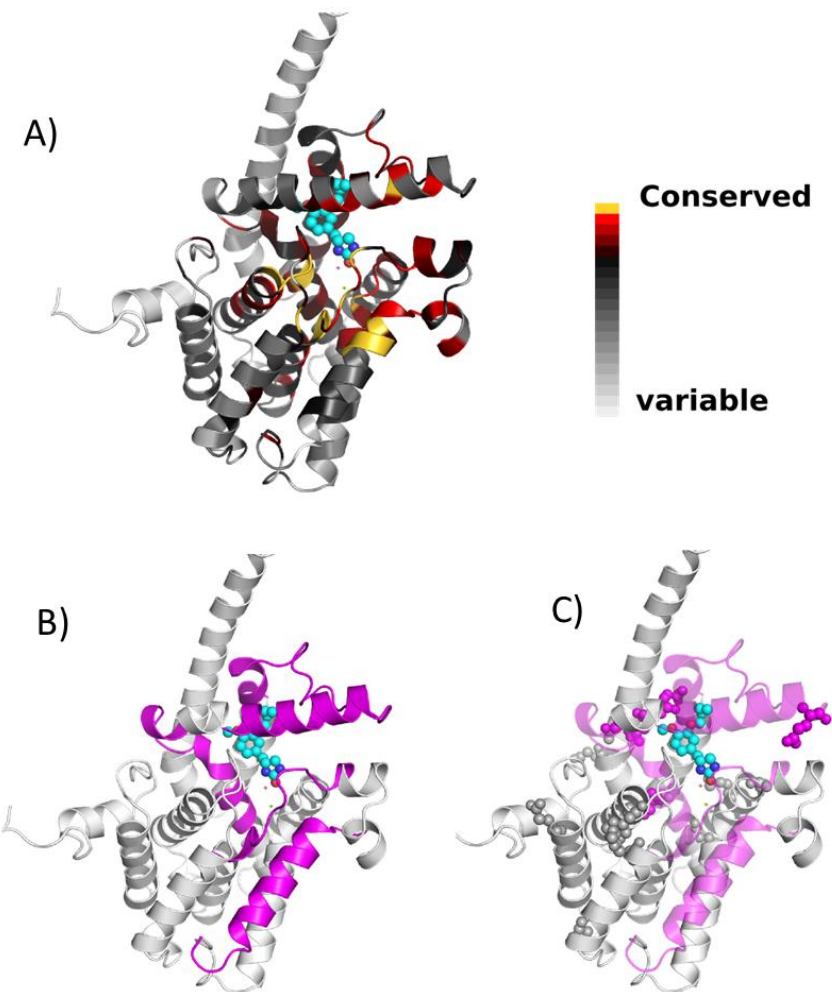
**Supplementary Figure S2: Mapping the interaction interface of RI $\alpha_A$  on RegAc by HDXMS:** A) Difference in HDXMS levels (y-axis) between free RegAc and in complex with RI $\alpha_A$  are plotted for the pepsin digest fragments (x-axis) analyzed in this study. Time points are represented in different colors; orange, brown, blue and black for 1, 2, 5 and 10 min respectively. Blue dotted boxes highlight the three regions (I, II and III) within RegAc showing decreased deuterium exchange in the PDE-RI $\alpha$  complex. Plots are the average from two independent HDX-MS experiment generated using the DynamX software (Version 2.0, Waters, Milford). B) ESI-QTOF mass spectra of pepsin digest fragments from different regions of RegAc that showed significant changes in amide H/D exchange upon interactions with RI $\alpha_A$ . (i) The isotopic envelope for the peptides from RegAc in the presence of RI $\alpha_A$  after 10 min deuteration (ii) The isotopic envelope for the peptides from RegAc in the absence of RI $\alpha_A$  after 10 min deuteration; (iii) undeuterated isotopic envelope of peptides from RegAc. C) Time course (1 - 10 min) of deuterium exchange for peptides from RegAc. Open circle (○), RegAc in the absence of RI $\alpha_A$ ; Close circle (●), RegAc in the presence of RI $\alpha$  (91-244).

## Supplementary Figure S3



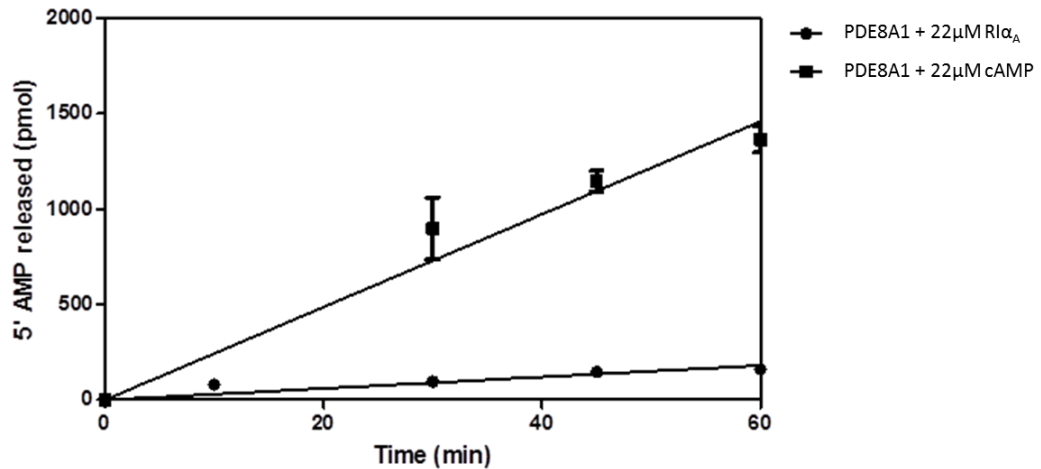
**Supplementary Figure S3:** Sequence homology of RegA across PDE superfamily (From ENSEMBL).

## Supplementary Figure S4



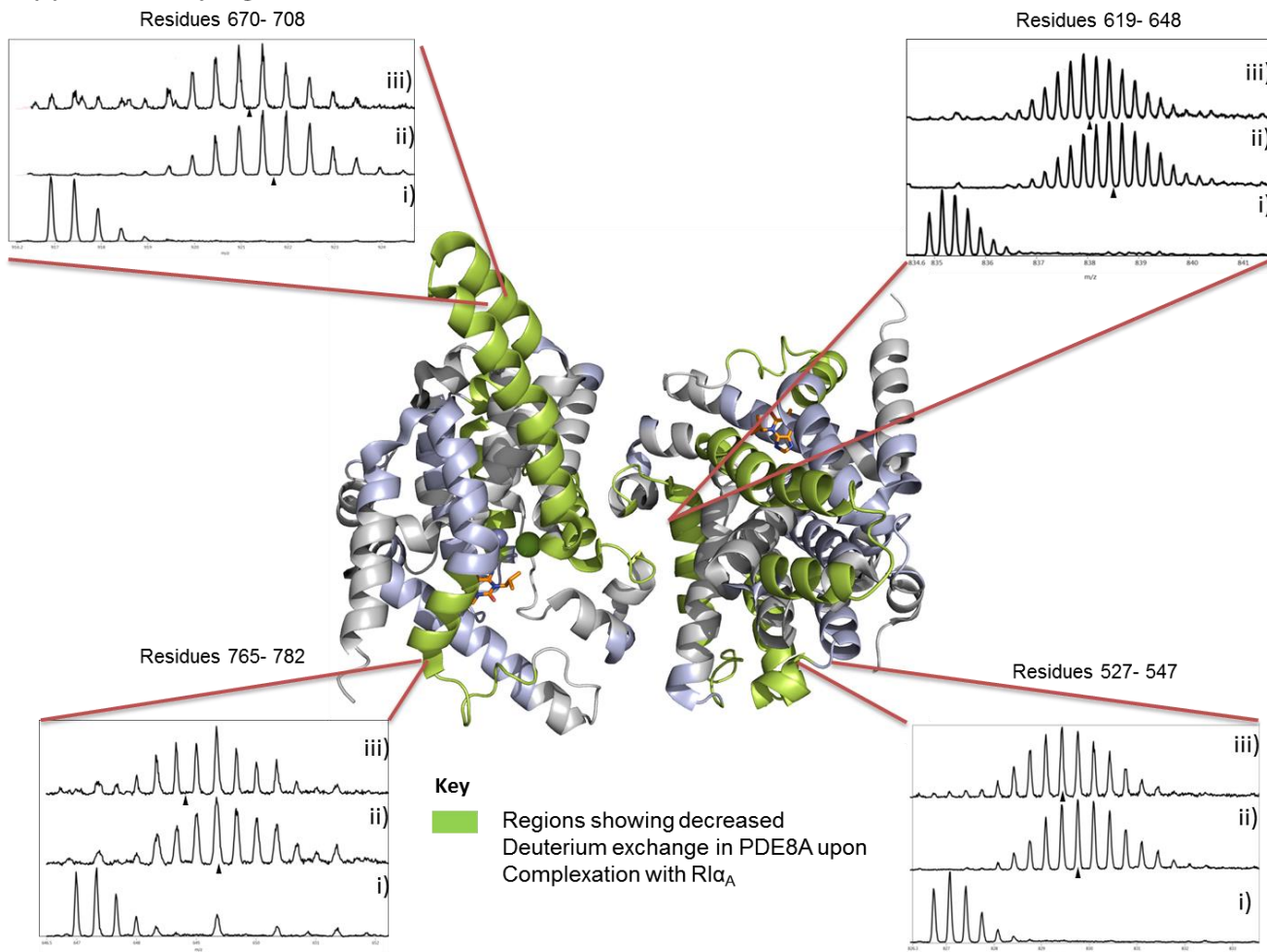
**Supplementary Figure S4:** Cartoon of PDE model structure A) color coded based on conservation index; B) regions that interact with RI $\alpha$  in magenta; C) discriminants as spheres. cAMP analogue is shown as blue spheres.

Supplementary Figure S5



**Supplementary Figure S5: PDE8A1 is capable of catalyzing hydrolysis of cAMP bound to RI $\alpha$ :** Phosphodiesterase activity was calculated using a phosphate coupled colorimetric assay based on hydrolysis of cAMP to AMP by phosphodiesterases coupled to the hydrolysis of AMP to inorganic phosphate by alkaline phosphatase. In this assay, catalytic amounts of PDE8A1 (50 nM) was incubated with 22  $\mu$ M of cAMP bound RI $\alpha$ <sub>A</sub> for different incubation times. Phosphodiesterase activity of PDE8A1 (50 nM) with 22  $\mu$ M of free cAMP was also carried out for comparison. The plot compares the amount of 5' AMP released (y-axis) with increasing labeling times (x-axis). The plot shows that PDE8A1 is capable of hydrolyzing cAMP bound to RI $\alpha$ <sub>A</sub> (■), albeit at a rate 8 times slower than rate of hydrolysis of PDE8A1 for free cAMP (●). The points were fit to a linear equation (Graphpad Prism version 5 (San Diego, CA)).

### Supplementary Figure S6



**Supplementary Figure S6: Map of the RI $\alpha$ <sub>A</sub> interaction interface on the catalytic domain of full-length PDE8A:** Effects of RI $\alpha$ <sub>A</sub> interactions with the catalytic PDE domain of full-length PDE8A by HDXMS is mapped onto the dimeric structure of PDE8A<sub>C</sub> (PDB ID: 3ECN). Regions of the PDE8A<sub>C</sub> that show significant reduction in deuterium exchange upon complex formation are colored green, regions showing no difference in exchange are white. Regions for which no coverage was obtained are in light blue. Mass spectra of peptides showing significant changes upon RI $\alpha$ <sub>A</sub> complex formation (Difference>1Da) are shown. The isotopic envelopes of pepsin fragment peptides of i) Undeuterated control of PDE8A ii) free PDE8A after 2 min deuteration iii) PDE8A in a complex with RI $\alpha$ <sub>A</sub> after 2 min deuteration are depicted. Centroids are indicated ( $\blacktriangle$ ).

## Supplementary Tables

**Supplementary table S T1:** Summary of H/D exchange data for free PDE8A<sub>C</sub> and PDE8A<sub>C</sub> bound to RIα<sub>A</sub>

No.	Pepsin Digest Fragments of PDE8A <sub>C</sub> (m/z)	Charge (z)	Residue nos.	Maximum Exchangeable amides	Maximum deuterons exchanged after 2 min	
					Free PDE8A <sub>C</sub> (mean ± SD)	PDE8A <sub>C</sub> : RIα <sub>AB</sub> complex (mean±SD)
1	DDVPPRIARA (555.303)	2	482-491	7	4.06 ± 0.01	3.79 ± 0.07
2	DDVPPRIARAME (685.344)	2	482-493	9	5.08 ± 0.00	4.66 ± 0.02
3	DDVPPRIARAMENE (801.887)	2	482-495	11	6.07 ± 0.02	5.60 ± 0.10
4	PPRIARA (390.741)	2	485-491	5	3.16 ± 0.02	2.70 ± 0.04
5	RIARAMENEYWFDFIFELEAATHNRPLIYLG (777.378)	5	487-518	30	6.72 ± 0.08	5.28 ± 0.04
6	ELEAATHNRPLIY (763.898)	2	504-516	11	0.79 ± 0.08	0.84 ± 0.05
7	ELEAATHNRPLIYL (820.44)	2	504-517	12	0.60 ± 0.05	0.67 ± 0.05
8	LEAATHNRPLIY (699.377)	2	505-516	10	0.67 ± 0.03	0.64 ± 0.04
9	LEAATHNRPLIYLGLKM (647.359)	3	505-521	15	0.55 ± 0.08	0.68 ± 0.04
10	EAATHNRPLIYL (699.377)	2	506-517	10	0.38 ± 0.06	0.48 ± 0.05
11	ATHNRPLIYL (599.337)	2	508-517	8	0.32 ± 0.03	0.34 ± 0.01
12	LGLKM (561.342)	1	517-521	4	0.21 ± 0.00	0.16 ± 0.04
13	FGICEFLHCSESTLRSWL (1064.499)	2	525-542	17	6.55 ± 0.04	4.67 ± 0.02

14	CSESTLRSWLQIIEAN (925.455)	2	533-548	15	$5.10 \pm 0.03$	$3.78 \pm 0.04$
15	QIIEANY (850.430)	1	543-549	6	$5.10 \pm 0.03$	$3.78 \pm 0.04$
16	ANYHSSNPYHNSTHSADVL (705.310)	3	547-565	17	$1.25 \pm 0.06$	$0.90 \pm 0.07$
17	NYHSSNPYHNSTHSADVL (681.631)	3	548-565	16	$1.06 \pm 0.06$	$0.80 \pm 0.00$
18	SNPYHNSTHSADVLHATA (641.293)	3	552-569	16	$2.51 \pm 0.09$	$1.68 \pm 0.03$
19	FLSKERIKE (575.331)	2	571-579	8	$1.81 \pm 0.03$	$1.47 \pm 0.06$
20	FLSKERIKETLDPIDE (645.009)	3	571-586	14	$3.03 \pm 0.10$	$2.66 \pm 0.05$
21	LSKERIKETLDPIDE (595.986)	3	572-586	13	$2.98 \pm 0.09$	$2.62 \pm 0.06$
22	RIKETLDPIDE (664.853)	2	576-586	9	$1.68 \pm 0.04$	$1.56 \pm 0.00$
23	TLDPIDE (802.382)	1	580-586	5	$1.07 \pm 0.00$	$1.02 \pm 0.01$
24	IAATIHDVDHPGRTNS (568.615)	3	591-606	14	$2.50 \pm 0.01$	$1.90 \pm 0.05$
25	IAATIHDVDHPGRTNSF (617.633)	3	591-607	15	$2.37 \pm 0.04$	$1.92 \pm 0.03$
26	IAATIHDVDHPGRTNSFL (655.332)	3	591-608	16	$2.29 \pm 0.03$	$1.81 \pm 0.04$
27	CNAGSELAILYNDT (742.336)	2	609-622	13	$2.66 \pm 0.04$	$1.91 \pm 0.10$
28	ESHHAAL (373.684)	2	626-632	6	$1.20 \pm 0.00$	$0.94 \pm 0.04$
29	ESHHAALA (418.202)	2	626-633	7	$1.62 \pm 0.01$	$1.29 \pm 0.02$
30	LTTGDDKCNIFKNM (800.375)	2	636-649	13	$2.85 \pm 0.01$	$2.05 \pm 0.01$
31	TGDDKCNIFKNMER (835.881)	2	638-651	13	$3.06 \pm 0.00$	$2.53 \pm 0.10$
32	KNMERNDY (535.236)	2	647-654	7	$2.37 \pm 0.03$	$1.91 \pm 0.07$
33	KNMERNDYRTLQRQIIDM (751.707)	3	647-664	17	$3.76 \pm 0.01$	$3.07 \pm 0.00$
34	RTLRQIID (536.313)	2	655-663	8	$1.16 \pm 0.01$	$1.14 \pm 0.06$

35	LRQGIID (814.478)	1	657-663	6	$0.64 \pm 0.00$	$0.60 \pm 0.01$
36	VLATE (532.297)	1	665-669	4	$0.59 \pm 0.01$	$0.67 \pm 0.04$
37	VLATEM (663.338)	1	665-670	5	$0.94 \pm 0.02$	$0.86 \pm 0.04$
38	VLATEMTKHFEHVNKFVNSINKPLAT (742.892)	4	665-690	24	$6.31 \pm 0.08$	$5.40 \pm 0.07$
39	ATEMTKHFEHVNKFVNSINKPLAT (689.854)	4	667-691	22	$5.31 \pm 0.10$	$4.67 \pm 0.03$
40	ATEMTKHFEHVNKFVNSINKPLATL (718.125)	4	667-692	23	$6.03 \pm 0.18$	$5.22 \pm 0.16$
41	MTKHFEHVNKF (473.235)	3	670-680	10	$1.23 \pm 0.04$	$1.05 \pm 0.04$
42	MTKHFEHVNKFVNS (573.282)	3	670-683	13	$1.87 \pm 0.08$	$1.50 \pm 0.02$
43	MTKHFEHVNKFVNSINKPLAT (819.097)	3	670-690	19	$4.84 \pm 0.10$	$4.29 \pm 0.04$
44	MTKHFEHVNKFVNSINKPLATL (856.792)	3	670-691	20	$5.41 \pm 0.07$	$4.72 \pm 0.04$
45	VNSINKPLAT (528.802)	2	681-690	8	$3.38 \pm 0.02$	$3.08 \pm 0.02$
46	INKPLAT (756.461)	1	684-690	5	$2.46 \pm 0.01$	$2.21 \pm 0.01$
47	INKPLATL (435.272)	2	684-691	6	$2.93 \pm 0.01$	$2.46 \pm 0.00$
48	LEENGETDKNQE (703.304)	2	691-702	11	$3.85 \pm 0.00$	$3.17 \pm 0.05$
49	LEENGETDKNQEINT (916.925)	2	691-707	15	$6.30 \pm 0.05$	$5.17 \pm 0.00$
50	LEENGETDKNQEINTM (982.445)	2	691-708	16	$6.49 \pm 0.09$	$5.20 \pm 0.02$
51	EENGETDKNQEINTM (925.903)	2	692-708	15	$5.99 \pm 0.08$	$4.82 \pm 0.01$
52	MLRTPENRTL (615.831)	2	707-716	8	$2.65 \pm 0.05$	$2.59 \pm 0.03$
53	LIKRML (387.253)	2	716-721	5	$0.42 \pm 0.01$	$0.41 \pm 0.04$

54	WAARISE ( <i>416.715</i> )	2	740-746	6	$0.35 \pm 0.00$	$0.55 \pm 0.02$
55	WAARISEE ( <i>481.236</i> )	2	740-747	7	$0.49 \pm 0.03$	$0.74 \pm 0.03$
56	YFSQTDE ( <i>889.357</i> )	1	748-754	6	$1.50 \pm 0.01$	$1.09 \pm 0.01$
57	YFSQTDEEKQQGLPVVM ( <i>999.974</i> )	2	748-764	15	$5.79 \pm 0.04$	$4.48 \pm 0.03$
58	FSQTDEEKQQGLPVVM ( <i>918.44</i> )	2	749-764	14	$6.19 \pm 0.03$	$4.70 \pm 0.02$
59	DEEKQQGLPVVM ( <i>686.839</i> )	2	753-764	10	$5.09 \pm 0.01$	$4.21 \pm 0.12$
60	EKQQGLPVVM ( <i>564.804</i> )	2	755-764	8	$4.17 \pm 0.03$	$3.34 \pm 0.04$
61	FITDM ( <i>626.285</i> )	1	785-789	4	$1.55 \pm 0.02$	$1.38 \pm 0.01$
62	FITDMF ( <i>773.353</i> )	1	785-790	5	$1.47 \pm 0.04$	$1.12 \pm 0.04$
63	FITDMFDAWDAFV ( <i>789.349</i> )	2	785-797	12	$2.56 \pm 0.03$	$2.13 \pm 0.02$
64	FDAWDA ( <i>724.293</i> )	1	790-795	5	$0.25 \pm 0.02$	$0.12 \pm 0.04$
65	FVDLPDL ( <i>818.429</i> )	1	796-802	5	$0.78 \pm 0.03$	$0.76 \pm 0.00$
66	VDLPDL ( <i>671.361</i> )	1	797-802	4	$0.68 \pm 0.02$	$0.61 \pm 0.02$
67	MQHLDNNF ( <i>509.7205</i> )	2	803-810	7	$0.72 \pm 0.03$	$0.57 \pm 0.01$
68	MQHLDNNFKYWKGGLDE ( <i>679.983</i> )	3	803-818	15	$2.15 \pm 0.09$	$1.91 \pm 0.01$
69	FKYWKGGLDE ( <i>593.297</i> )	3	810-818	8	$1.79 \pm 0.04$	$1.65 \pm 0.01$

**Supplementary table S T2:** Summary of H/D exchange data for free RI $\alpha_{AB}$  and RI $\alpha_{AB}$  bound to PDE8A<sub>C</sub>

No.	Pepsin Digest Fragments of RI $\alpha_{AB}$ (m/z)	Charge (z)	Residue nos.	Maximum Exchangeable amides	Maximum deuterons exchanged after 2 mins	
					Free RI $\alpha_{AB}$ (mean±SD)	RI $\alpha_{AB}$ : PDE8A <sub>C</sub> complex (mean±SD)
1	EISPPPPNPV (523.775)	2	79-88	4	2.8 ± 0.15	1.9 ± 0.03
2	AISAE (490.215)	1	97-101	4	1.5 ± 0.02	1.1 ± 0.02
3	AEVYTEE (840.362)	1	100-106	6	2.5 ± 0.1	2.4 ± 0.04
4	YVRKVIPKDYKTM (547.64)	3	111-123	11	5.4 ± 0.08	4.8 ± 0.09
5	YVRKVIPKDYKTMAA (594.996)	3	111-125	13	6.5 ± 0.18	5.8 ± 0.09
6	VRKVIPKDYKTMAA (540.643)	3	112-125	12	6.1 ± 0.1	5.6 ± 0.09
7	LAKAIEKNV (493.604)	2	126-134	8	3.7 ± 0.08	2.7 ± 0.04
8	LAKAIEKNVL (549.845)	2	126-135	9	4.3 ± 0.07	3.3 ± 0
9	FSHLDDNE (488.700)	2	136-143	7	1.4 ± 0.01	1.1 ± 0.02
10	RSDIF (637.33)	1	144-148	4	0.6 ± 0.04	0.2 ± 0.01
11	DAMFPVSF (913.412)	1	149-156	6	1.3 ± 0	1.1 ± 0.04
12	FPVSF (596.308)	1	153-156	3	1.1 ± 0	0.7 ± 0
13	IAGET (490.251)	1	157-161	4	1 ± 0.02	0.8 ± 0.01
14	FYVIDQGEM (1101.49)	1	172-180	8	2.2 ± 0.05	1.1 ± 0.01
15	FYVIDQGEMDV (1315.59)	1	172-182	10	2.8 ± 0.13	1.4 ± 0.1

16	YVIDQGEMDV ( <i>1168.519</i> )	1	173-182	9	$2.4 \pm 0.06$	$1.5 \pm 0.04$
17	DVYVNNE ( <i>852.3734</i> )	1	181-187	6	$2.2 \pm 0.04$	$1.5 \pm 0.02$
18	YVNNE ( <i>638.278</i> )	1	183-187	4	$1.5 \pm 0.02$	$1.4 \pm 0.04$
19	WATSVGEGGSFGEL ( <i>698.818</i> )	2	188-201	13	$5.3 \pm 0.10$	$3.0 \pm 0.02$
20	ALIYGTTPRAAT ( <i>567.315</i> )	2	202-212	9	$4.9 \pm 0.05$	$3.4 \pm 0.04$
21	ALIYGTTPRAATVKAKTNVKL ( <i>705.753</i> )	3	202-221	18	$8.0 \pm 0.16$	$4.9 \pm 0.01$
22	LIYGTTPRAATVKAKTNVVK ( <i>644.38</i> )	3	203-220	16	$7.4 \pm 0.17$	$4.2 \pm 0.08$
23	YGTTPRAATVKAKTNVKL ( <i>606.686</i> )	3	205-221	15	$6.7 \pm 0.20$	$4.4 \pm 0.03$
24	VKAkTNVKL ( <i>500.825</i> )	2	213-221	8	$2.6 \pm 0.04$	$1.8 \pm 0.02$
25	WGIDRDSY ( <i>506.225</i> )	2	221-229	7	$1.6 \pm 0.03$	$0.8 \pm 0.00$
26	RRILMGST ( <i>467.265</i> )	2	230-237	7	$2.6 \pm 0.02$	$2.0 \pm 0.10$
27	RRILMGSTL ( <i>523.805</i> )	2	230-238	8	$3.1 \pm 0.04$	$1.9 \pm 0.01$
28	FLSKVSIL ( <i>453.793</i> )	2	247-254	7	$3.0 \pm 0.14$	$2.4 \pm 0.01$
29	LSKVSIL ( <i>759.497</i> )	1	248-254	6	$2.6 \pm 0.06$	$2.1 \pm 0$
30	SKVSIL ( <i>646.413</i> )	1	249-254	5	$2.4 \pm 0.02$	$1.9 \pm 0.00$
31	TVADALE ( <i>718.361</i> )	1	264-270	6	$3.0 \pm 0.09$	$2.2 \pm 0.04$
32	ADALEPVQFEDGQ ( <i>709.82</i> )	2	266-278	11	$5.3 \pm 0.15$	$1.8 \pm 0.00$
33	DALEPVQF ( <i>918.456</i> )	1	267-274	6	$2.8 \pm 0.06$	$1.5 \pm 0.00$
34	PVQFEDGQKIVVQGEPEGDEF ( <i>1109.535</i> )	2	271-290	18	$5.5 \pm 0.09$	$2.6 \pm 0.04$
35	EDGQKIVVQGEPEGDEF ( <i>873.91</i> )	2	275-290	14	$4.4 \pm 0.07$	$2.1 \pm 0.01$
36	IVVQGEPEGDEFF ( <i>668.82</i> )	2	280-291	10	$4.1 \pm 0.08$	$2.7 \pm 0.05$
37	IILEGSA ( <i>702.403</i> )	1	292-298	6	$1.1 \pm 0.02$	$0.9 \pm 0.00$

38	QRRSENEE (524.24)	2	302-309	7	$2.4 \pm 0.06$	$1.9 \pm 0.05$
39	QRRSENEEF (597.775)	2	302-310	8	$2.5 \pm 0.05$	$2.2 \pm 0.01$
40	FVEVGRLGPSDY (669.835)	2	310-321	10	$3.0 \pm 0.06$	$1.6 \pm 0.01$
41	VEVGRLGPSDY (596.3)	2	311-321	9	$2.4 \pm 0.04$	$1.5 \pm 0.07$
42	LGPSDYFGEI (549.26)	1	316-325	8	$4.6 \pm 0.05$	$3.2 \pm 0.00$
43	FGEIAL (649.355)	1	322-327	5	$2.3 \pm 0.04$	$0.8 \pm 0.01$
44	LMNRPRAAT (1029.562)	2	328-336	7	$3.3 \pm 0.02$	$1.6 \pm 0.01$
45	MNRPRAAT (458.739)	2	329-336	6	$3.1 \pm 0.04$	$1.4 \pm 0.04$
46	ARGPLKCV (422.243)	2	339-346	6	$1.2 \pm 0.07$	$0.8 \pm 0.07$
47	VKLDRPRF (515.805)	2	346-353	6	$2.2 \pm 0.05$	$1.2 \pm 0.02$
48	LDRPR (328.692)	2	348-352	3	$1.6 \pm 0.01$	$0.9 \pm 0.01$
49	ERVLGPCSDIL (601.31)	2	354-364	9	$3.8 \pm 0.01$	$1.6 \pm 0.01$

## Supporting References

- Burns-Hamuro, L. L., Y. Ma, S. Kammerer, U. Reineke, C. Self, C. Cook, G. L. Olson, C. R. Cantor, A. Braun, and S. S. Taylor. 2003. Designing isoform-specific peptide disruptors of protein kinase A localization. Proceedings of the National Academy of Sciences of the United States of America 100:4072-4077.
- Sathyanarayana, P., E. Houde, D. Marshall, A. Volk, D. Makropoulos, C. Emerson, A. Pradeep, P. J. Bugelski, and D. M. Wojchowski. 2009. CNTO 530 functions as a potent EPO mimetic via unique sustained effects on bone marrow proerythroblast pools. Blood 113:4955-4962.
- Bogacheva, O., O. Bogachev, M. Menon, A. Dev, E. Houde, E. I. Valoret, H. M. Prosser, C. L. Creasy, S. J. Pickering, E. Grau, K. Rance, G. P. Livi, V. Karur, C. L. Erickson-Miller, and D. M. Wojchowski. 2008. DYRK3 dual-specificity kinase attenuates erythropoiesis during anemia. J Biol Chem 283:36665-36675.
- Moorthy, B. S., Y. Gao, and G. S. Anand. 2011. Phosphodiesterases catalyze hydrolysis of cAMP-bound to regulatory subunit of protein kinase A and mediate signal termination. Molecular & cellular proteomics : MCP 10:M110 002295.
- Mandell, J. G., A. Baerga-Ortiz, S. Akashi, K. Takio, and E. A. Komives. 2001. Solvent accessibility of the thrombin-thrombomodulin interface. Journal of molecular biology 306:575-589.

6. Houde, D., S. A. Berkowitz, and J. R. Engen. 2011. The utility of hydrogen/deuterium exchange mass spectrometry in biopharmaceutical comparability studies. *Journal of pharmaceutical sciences* 100:2071-2086.
7. Arnold, K., L. Bordoli, J. Kopp, and T. Schwede. 2006. The SWISS-MODEL workspace: a web-based environment for protein structure homology modelling. *Bioinformatics* 22:195-201.
8. Wang, H., Z. Yan, S. Yang, J. Cai, H. Robinson, and H. Ke. 2008. Kinetic and structural studies of phosphodiesterase-8A and implication on the inhibitor selectivity. *Biochemistry* 47:12760-12768.
9. Wojchowski, D. M., M. P. Menon, P. Sathyanarayana, J. Fang, V. Karur, E. Houde, W. Kapelle, and O. Bogachev. 2006. Erythropoietin-dependent erythropoiesis: New insights and questions. *Blood cells, molecules & diseases* 36:232-238.
10. Pikitch, E. K., C. Santora, E. A. Babcock, A. Bakun, R. Bonfil, D. O. Conover, P. Dayton, P. Doukakis, D. Fluharty, B. Heneman, E. D. Houde, J. Link, P. A. Livingston, M. Mangel, M. K. McAllister, J. Pope, and K. J. Sainsbury. 2004. Ecology. Ecosystem-based fishery management. *Science* 305:346-347.